



**MEASUREMENTS OF NEUTRON INDUCED SURFACE AND BULK
DEFECTS IN 4H SILICON CARBIDE**

THESIS

Kent T. Jones, Major, USA

AFIT/GNE/ENP/02M-03

**DEPARTMENT OF THE AIR FORCE
AIR UNIVERSITY
AIR FORCE INSTITUTE OF TECHNOLOGY**

Wright-Patterson Air Force Base, Ohio

APPROVED FOR PUBLIC RELEASE; DISTRIBUTION UNLIMITED.

The views expressed in this thesis are those of the author and do not reflect the official policy or position of the United States Air Force, Department of Defense, or the U. S. Government.

AFIT/GNE/ENP/02M-03

**MEASUREMENTS OF NEUTRON INDUCED SURFACE AND BULK
DEFECTS IN 4H SILICON CARBIDE**

THESIS

Presented to the Faculty of the Graduate School of Engineering and Management

of the Air Force Institute of Technology

Air University

In partial fulfillment of the requirements for the degree of

Master of Science in Nuclear Engineering

Kent T. Jones, B.S. EE

Major, USA

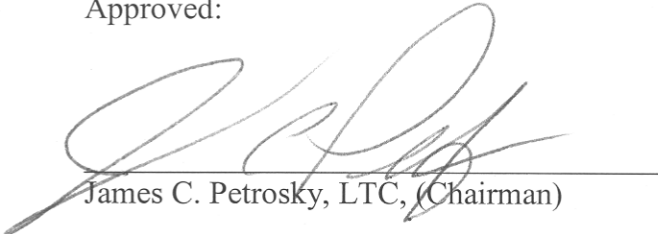
March 2002

APPROVED FOR PUBLIC RELEASE; DISTRIBUTION UNLIMITED.

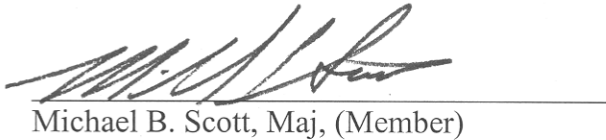
**MEASUREMENTS OF NEUTRON INDUCED SURFACE AND BULK
DEFECTS IN 4-H SILICON CARBIDE**

Kent T. Jones, B.S. EE
Major, USA


Approved:


James C. Petrosky, LTC, (Chairman)

08 MAR 02
date


Michael B. Scott, Maj, (Member)

8 MAR 02
date


Larry W. Burggraf, (Member)

5 Mar 02
date

Acknowledgements

I would like to express my appreciation to LTC Petrosky and Mr. Greg Smith of the AFIT Engineering Physics Department for their guidance and support to my efforts during this project. Without their expertise I would have been lost many times during the course of my work.

I would like to thank Joe and the professional staff at The Ohio State University Fission Reactor for their assistance. Their professionalism was critical to the success of this research. Reactor use was sponsored by the U.S. Department of Energy, through the “Reactor Sharing Program” under grant number: DE-FG02-95NE38120.

Also, I would like to thank my classmates whose constant support and critical review will always be treasured.

Kent T. Jones

“We’ve got a heavy task before us.” - BG John Buford, Commander, 1st Cavalry Division, Army of the Potomac, in conveying deployment orders to his commanders on Cash Town Pike west of Gettysburg, Pennsylvania, 30 June 1863.

Table of Contents

	Page
Acknowledgements	ii
List of Figures	v
List of Tables.....	vii
Abstract	viii
I. Introduction.....	1
Background	1
Problem Statement	2
Scope	2
General Approach.....	2
II. Background.....	4
Features of the Crystal Structure of SiC.....	4
Electrical Properties of Silicon Carbide	6
Neutron Radiation Effects on Semiconductors	8
III. Experiment	13
Experimental Procedure	13
Neutron Irradiation	14
Device Fabrication	16
Sample Analysis Techniques	19
Photoluminescence (PL)	19
Constant Voltage Deep Level Transient Spectroscopy (CV-DLTS)	22
Hall Effect Measurements (HALL).....	30
IV. Results.....	34
N- Type Silicon Carbide	34
n-type Photoluminescence Results.....	34
n-type DLTS Results.....	38
n-type Hall Results.....	44
P-Type Silicon Carbide	47
p-type Photoluminescence Results.....	47
p-type DLTS Results	49
p-type Hall Results.....	54
Other Observations.....	57
V. Research Summary.....	60
Conclusions	60
Photoluminescence.....	60

Deep Level Transient Spectroscopy.....	61
Hall effect.....	61
Applications	61
Recommendations for Future Research	62
Appendix A: Irradiation Test Plan	64
Introduction	64
Background	64
Bulk 4H Silicon Carbide	64
Radiation Source	67
Test Objectives.....	68
Test Description	68
Sample Preparation	68
Actions at Reactor Site.....	68
Post Irradiation Handling	69
Test Priorities	69
Radiation and Safety and Activation.....	70
Safety Plan.....	70
Travel Plan	71
Post-Irradiation Analysis Plan.....	71
Points of Contact	71
Irradiation Calculations	73
Experimental Equipment.....	84
Sample Preparation and Wafer Utilization.....	85
Sample Preparation List	85
Wafer Utilization Plan.....	86
Appendix B: Device Fabrication.....	89
Sample Clean.....	89
Wafer Cut & Mark	89
Oxide Acid Etch	90
Ohmic Backside Contacts	90
Ohmic van der Pauw Contacts	90
Contact Anneal	91
Rectifying Schottky Contacts.....	91
Bibliography.....	93
Vita	96

List of Figures

	Page
Figure 1: Schematic Cross-Section {(1120) plane} of 4H-SiC Polytype	6
Figure 2: Creation of Electron-Hole Pairs due to Ionizing Radiation.....	9
Figure 3: Formation of Defect Sites by Neutron Bombardment.....	11
Figure 4: OSURR Reactor Fission Spectrum.....	15
Figure 5: Two-Sided Schottky Diode for DLTS Experiment	18
Figure 6: van der Pauw Contact for Hall Effect Experiment	18
Figure 7: PL Spectrum from an Unirradiated n-type 4H-SiC Sample	20
Figure 8: Radiative Transitions Observed with PL.....	21
Figure 9: Typical Photoluminescence Experimental Setup	22
Figure 10: Measured DLTS Spectrum of Irradiated 4H-SiC	26
Figure 11: Capacitance Transients at Various Temperatures.....	27
Figure 12: Measured Arrhenius Plot from Irradiated 4H-SiC.....	28
Figure 13: Typical DLTS Setup.....	29
Figure 14: Arrhenius Plot Analysis Software Interface	30
Figure 15: Illustration of Hall Effect in a p-type Sample.....	31
Figure 16: Typical Hall Set Up	33
Figure 17: PL Spectrum for Un-irradiated n-type 4H Silicon Carbide.....	35
Figure 18: Observed PL Peaks in n-type 4H SiC.....	36
Figure 19: PL Response of n-type SiC to various Irradiation Levels	37
Figure 20: DLTS Rate Window Response of Damaged n-type SiC.....	39
Figure 21: Arrhenius Plot Depiction of one Trap Site	40
Figure 22: Observed Capacitance Roll-Over in Irradiated 4H-SiC	42
Figure 23: Resistivity vs. Fluence in n-type SiC.....	44
Figure 24: Sheet Carrier Concentration vs. Fluence for n-type SiC	45
Figure 25: Hall Mobility vs. Fluence for n-type SiC	46
Figure 26: Hall Coefficient vs. Fluence for n-type SiC	47
Figure 27: Un-irradiated PL Spectrum of p-type 4H Silicon Carbide	48
Figure 28: PL Response of p-type SiC to Various Irradiation Levels	49

Figure 29: Measured DLTS Response of Irradiated p-type SiC	50
Figure 30: Measured I-V Curve of Un-irradiated p-type 4H SiC Schottky Diode	51
Figure 31: Back-Side Ohmic Contact on p-type SiC	52
Figure 32: Measured Capacitance vs. Temperature Curve of p-type SiC.....	53
Figure 33: Measured Resistivity vs. Fluence for p-type SiC	55
Figure 34: Measured Sheet Carrier vs. Fluence for p-type SiC	56
Figure 35: Measured Hall Mobility vs. Fluence for p-type SiC.....	56
Figure 36: Measured Hall Coefficient vs. Fluence for p-type SiC.....	57
Figure 37: Measured I-V Curve for an Irradiated p-type Schottky Diode	59
Figure 38: Measured Carrier Concentration Profile for a n-type Schottky Diode	59
Figure 39: OSU Reactor Core	84
Figure 40: Ohmic van der Pauw Contacts (under mask)	91
Figure 41: Rectifying Schottky Contacts	92

List of Tables

	Page
Table 1: Comparison of Silicon Carbide Properties to Silicon and Gallium Arsenide.....	7
Table 2: Experimental Material Characteristics.....	13
Table 3: Required Preparation of Samples.....	17
Table 4: Reported Energy of ZPL Phonon Replicas for 4H-SiC	36
Table 5: n-type 4H-SiC DLTS Results	40
Table 6: Dopant Level vs. Neutron Fluence in n-type SiC at Room Temp	43
Table 7: Measured Dopant Level vs. Neutron Fluence in p-type SiC	54
Table 8: Measured Schottky Diode Leakage Current in n-type 4H SiC.....	58
Table 9: Bulk Sample Study.....	66
Table 10: Irradiation Targets.....	67

Abstract

The effects of neutron irradiation was investigated in both n- and p-type 4H silicon carbide. Photoluminescence (PL), deep level transient spectroscopy (DLTS), and Hall effect measurements were used to observe optical and electrical characteristics and identify changes in basic material properties. The material was irradiated using an open pool research reactor. Highly doped n- and p-type materials ($N_D-N_A \sim 1.2E17$ and $N_A-N_D \sim 1.5E18 \text{ cm}^{-3}$ respectively) were chosen to aid in device fabrication.

The material demonstrated no measurable effect to 1 MeV neutrons at fluences of up to $1E14 \text{ n/cm}^2$ and devices were unable to be constructed when exposed to fluences greater than $1E16 \text{ n/cm}^2$. The effective suppression of the near bandgap zero phonon PL luminescence lines was shown as a function of increasing neutron fluence, and attributed to the dislocation of neutral nitrogen donors. Deep level defects sites also developed and were shown to increase in density with increased neutron fluence. Hall measurements generally agreed with theoretical expectations but failed to yield conclusive results. Capacitance rollover was observed near 510 K beginning with fluences of around $5E15 \text{ n/cm}^2$. Irradiated devices also showed unexpectedly permanent degradation after hour-long exposure to temperatures exceeding 600K during DLTS measurements.

MEASUREMENTS OF NEUTRON INDUCED SURFACE AND BULK DEFECTS IN 4H SILICON CARBIDE

I. Introduction

Background

As electronic devices play an ever-increasing role in almost every type of machine, we are demanding increased performance in a variety of environments never thought of before. Traditional silicon devices are reasonably priced and are of generally good quality for most uses, but have drawbacks such as poor neutron hardness, which make them undesirable for many applications such as space-based electronics and nuclear weapon defense. To fill the semiconductor demand in these harsh environments, different materials and robust devices are being developed. These include gallium arsenide (GaAs), silicon-on-sapphire (SoS), and silicon carbide (SiC). Silicon carbide is desirable because of its electrical and mechanical properties, which allow it to perform at high-power and in both high-temperature and high-radiation environments where more traditional semiconductors fail (Neudeck, 2). The same properties that give SiC its physical hardness make it particularly resistant to the effects of neutron damage (Harris, ix). It is probable that SiC, in particular 4H-SiC, will play a significant role in future US projects such as the National Missile Defense (NMD) Project which require devices to perform in a neutron rich environment. Accurate measurements of neutron damage effects will allow device designers and manufacturers to correctly model device performance and to predict if devices made from this substrate do in fact meet their requirements or other material selections should be made.

Problem Statement

The goal of this thesis is to investigate changes in surface and bulk parameters following the neutron irradiation of 4H grown silicon carbide. This thesis will also examine the nature of measured defects and the influence of neutron radiation on devices fabricated from the material.

Scope

This research examines as-grown and irradiated 4H-SiC that has been irradiated over a range of neutron fluences. Measurements are made using three primary laboratory techniques: photoluminescence (PL), deep level transient spectroscopy (DLTS) and Hall effect measurements. Experimental results are analyzed and conclusions are drawn as a result of these measurements.

General Approach

This research project consists of numerous steps beginning with the receipt of four two-inch diameter 4H-SiC wafers. These wafers were initially inspected and visually mapped using a cross-polarizing filter. The wafers were then cut into 5 x 5 mm samples for irradiation, test device fabrication, and analysis.

A material irradiation test plan was then developed which describes the precise details of the neutron-irradiation experiment (Appendix A). The irradiation portion of the project was conducted at the research nuclear reactor at The Ohio State University. The test plan includes all handling procedures and all calculations required to reach the target irradiation levels. Target levels were selected following a thorough literature review, in an effort to produce consistent data over a range of values from nominal irradiation up to the expected material bandgap breakdown point (McLean *et al.*, 1994). Initial testing of

the irradiated samples confirmed the correctness of the chosen fluence range. The test plan also contains transportation requirements, special material handling requirements, dosimetry plan, and post irradiation test plans.

Both as-grown control samples and irradiated test samples were subsequently fabricated into the different test devices required for the chosen characterization techniques. Several manufacturing techniques and metal contact options were analyzed. The acceptable solution was based the ability to create quality ohmic and rectifying given the specific dopant level of the samples and availability of the contact metals.

The test devices were used to determine the electrical and optical characteristics of the material as a function of irradiation. The results of the experiments were then used to form conclusions about neutron-induced material defects.

II. Background

The Marconi Company first researched silicon carbide in 1907; their work is the first documented mention of the material's electro-luminescence properties. This initial work went unnoticed for almost 50 years until 1955 when Lely developed a growth method that produced nearly pure crystal samples. He grew single crystals by sublimation as a result of distilling SiC through a hot vapor phase into colder regions (Lebedev, 107). This breakthrough led to renewed interest in the material and the beginning of numerous conferences and publications detailing various properties of known SiC polytypes throughout the world. Interest in SiC soon waned again as technological difficulties in growing larger samples and fabricating devices resulted in performances that deviated widely from theoretically expected values. Research slowly continued as production difficulties were resolved and repeatable quality material was produced. Of the more than 140 SiC polytypes, several have received the greatest attention due to their desirable properties and ease of growth, which make them logical choices for device fabrication. Today high-quality production-grade SiC is available from manufactures such as Cree Research, Inc.

Features of the Crystal Structure of SiC

Silicon carbide is a striking representation of a polytype crystal. The term "polytypism" was introduced for carborundum, an early relative of SiC, and applied to SiC. This is because the different crystalline forms of SiC are structurally very close to one another, and differ only in the relative stacking of their silicon-carbon bi-layers. SiC is defined as a column IV-IV compound, meaning that both elements come from column

IV of the periodic table and thus have four valence shell electrons, which combine to form a tetrahedral covalent bond. Due to the bond type and length, SiC structures are relatively strong and are closely related to the strongest crystalline structures known (Sze, 11).

All the known polytypes of SiC crystallize in accordance with the close spherical packing law and are binary structures constructed of identical layers differing both in the order of positioning of the cubic C or hexagonal H layer and in the number of layers per unit cell. Each polytype can be characterized using the Ramsdell notation, which consists of a natural number (0,1,2, ...) equal to the number of bi-layers per period in the direction perpendicular to the basal plane and a single letter characterizing the orientation of the Bravais lattice: C for cubic, H for hexagonal, and R for rhombohedral. In 4H-SiC we have 4 layers per unit cell and a hexagonal lattice structure. The most common polytypes are 6H, 4H, 15R, and 3C. Although the position of the closest neighboring atoms is the same for each atom of silicon or carbon in all polytypes, the position of the next nearest neighbors is different. This leads to the appearance of crystallographically nonequivalent sites in the SiC lattice. For example 4H-SiC has one cubic (k) and one hexagonal (h) site while 6H-SiC with two cubic and one hexagonal (Lebedev, 108). Figure 1 illustrates the bi-layer stacking sequence and is one representation of the key elements in a 4H-SiC lattice (Lebedev, 109). The labels A, B, and C correspond to different stacking layers in a dense packed hexagonal structure. The symbols h and k denote hexagonal and cubic sites of SiC in the lattice, respectively.

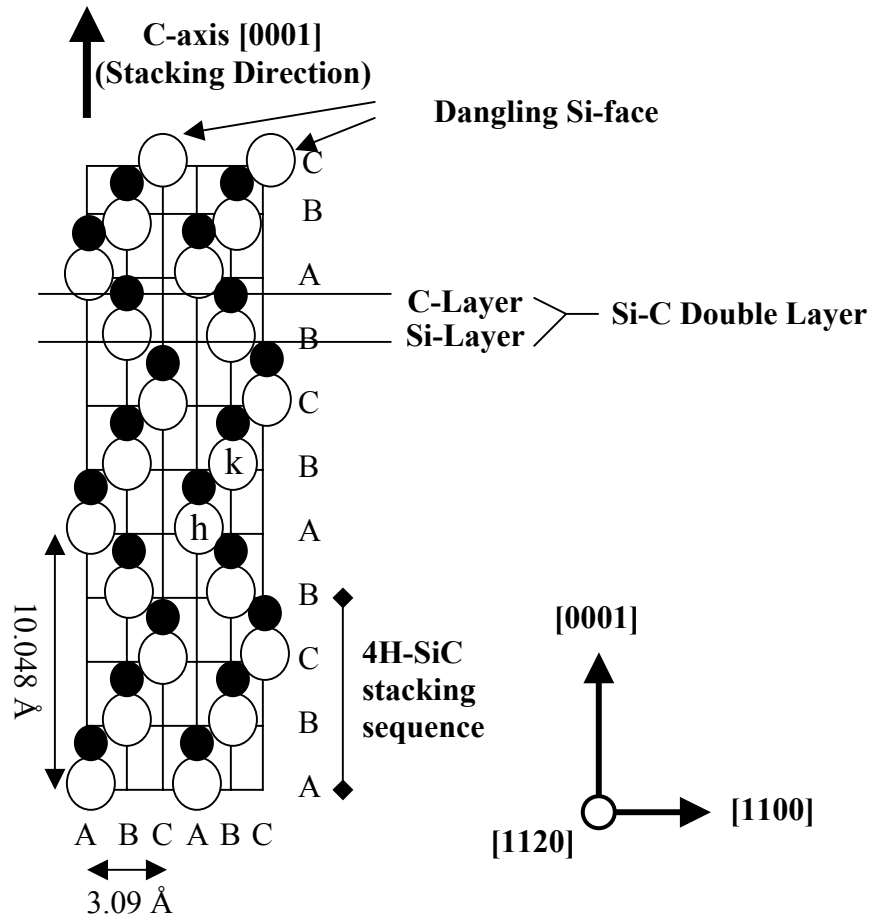


Figure 1: Schematic Cross-Section {(1120) plane} of 4H-SiC Polytype

Silicon carbide is an indirect bandgap semiconductor. Indirect bandgap semiconductors require a change in crystal momentum for an electron to transition from the valence to the conduction band. The bandgap structure is very important for light-emitting diodes and semiconductor lasers, which require direct bandgap semiconductors for efficient generation of photons (Sze, 14).

Electrical Properties of Silicon Carbide

Silicon carbide, in particular 4H SiC, has several numerical and electrical properties, which make it highly desirable for certain specialty applications such as high-

temperature, high-power, and/or high-radiation conditions (Neudeck, 2). Table 1 provides a comparison of several semiconductor properties that determine device performance (Scott, II-7).

Table 1: Comparison of Silicon Carbide Properties to Silicon and Gallium Arsenide

Property	Si	GaAs	3C-SiC	4H-SiC	6H-SiC
Bandgap (eV @RT)	1.1	1.4	2.2	3.2	2.9
Lattice Constant-a (Angstroms @RT)	5.43	5.65	4.36	3.08	3.08
Max. Operating Temperature (K)	600	760	1200	1740	1580
Electron/Hole Mobility RT, cm ² /Vs	1400/600	8500/400	1000/40	720/40	600/40
Breakdown Field 10 ⁶ V/cm (@ 10 ³ V)	0.3	0.4	2.3	4	3
Thermal Conductivity W/cm	1.5	0.5	4.9	4.9	4.9
Electron Saturation Velocity 10 ⁷ cm/s	1	2	2.5	2.2	2
Dielectric Constant K	11.8	12.8	9.7	9.7	9.7
Intrinsic Carrier Concentration (cm ⁻³ @RT)	10 ¹⁰	1.8*10 ⁶	10	10 ⁻⁷	10 ⁻⁵

To different degrees, SiC polytypes exhibit advantages and disadvantages in basic material properties as compared to silicon. The most beneficial inherent material advantages of SiC are: 1) the high breakdown electric field, which allows the device to carry a greater power load, 2) wide band gap energy, which can be more resistant to small voltage transients, 3) high thermal conductivity, which can bleed away internal heat faster and, 4) high carrier saturation velocity, which allows faster device switching.

If semiconductors are operated at relatively low temperatures, the induced dopant behavior will dominate the intrinsic carriers and the device will operate properly. As

temperature rises however, the intrinsic carriers become more energetic and may begin to transition the bandgap causing device failure so the significantly lower intrinsic carrier concentration is also a plus (Neudeck, 7). The low intrinsic carrier concentration also helps make SiC much less susceptible to ionizing radiation and there simple is less free charge available to interact. The wide bandgap and low intrinsic carrier concentration of SiC allow it to maintain proper semiconductor behavior at much higher temperatures (1740 K) than silicon (600 K).

The high breakdown field and high thermal conductivity of SiC, coupled with high operational junction temperatures permit high power densities and greater thermal efficiencies to be realized in SiC devices. Thus strong fields can be generated and stored, and switching energy loss can be minimized through faster device response times and reduced heat build up. These features allow SiC to theoretically handle large loads and/or reduce overall circuit size.

Neutron Radiation Effects on Semiconductors

There are five primary ionizing radiation sources and environments: space, materials containing trace radioactive elements, nuclear explosion, nuclear reactor, and integrated circuit processing (Srouf *et al*, 6). Space radiation is naturally occurring and is of concern for both earth-orbiting satellites and deep space probes. Materials containing trace radioactive elements such as uranium are also naturally occurring and are of potential risk to semiconductors. Man-made sources of radiation are nuclear reactors, nuclear explosions and certain equipment routinely used in circuit processing such as x-ray and electron-beam lithography equipment.

Each of these environments contains a variety of potential irradiating sources: neutrons, gamma rays, x-rays, electrons, protons, alpha particles, ions, and cosmic rays. These are frequently grouped in terms of their damage mechanisms, as they are either charged, which react predominantly with the electrons in the columbic shell of the semiconductor (ionizing), or they are neutral, which react mainly with the nucleus of the atoms (non-ionizing).

Ionizing radiation effects result from high-energy charged particles; such as electrons, protons, ions, and alpha particles. As the particle passes through a semiconductor material, its columbic interaction disturbs bound electrons and may create electron-hole pairs. Figure 2 shows the creation of electron-hole pairs along the ionizing radiation particle path.

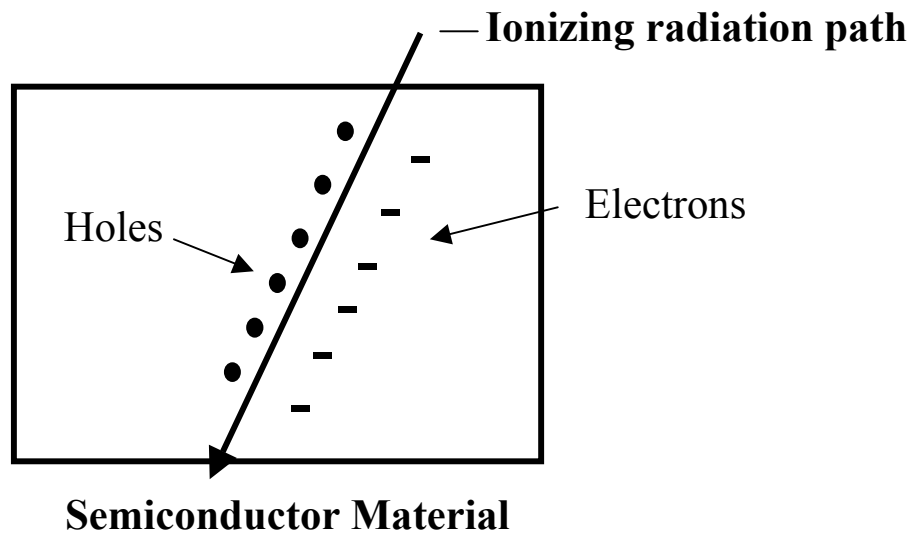


Figure 2: Creation of Electron-Hole Pairs due to Ionizing Radiation

The magnitude of the effect of electron-hole pairs on a device's performance is a function of; 1) the number created, 2) the rate at which they are produced, 3) the

electrical state of the device at the time of occurrence, and 4) the degree to which they recombine. If the number created is small and no field is present at the time of exposure, the electron-hole pairs will most likely recombine and the device will quickly return to its original state. If, however, a large number of electron-holes pairs are created in a short period, or a field is present at the time of exposure, the electrons may be unable to locate free holes and device degradation may become semi-permanent. This effect is especially true when interface effects are examined as the electron-hole pairs can migrate to the interface and cause a variety of additional problems (Ma *et al*, 485).

More permanent dislocation effects may be caused by non-ionizing radiation such as neutrons. Energetic neutrons can readily pass through a columbic shell retaining their energy until encountering the nucleus of an atom. Protons and heavy ions can also do this but frequently will interact with the columbic shell and loose some energy in that exchange. Thus one of the principle causes of permanent radiation damage to electronic systems is neutrons (Messenger *et al*, 197). Neutrons are relatively heavy, having a mass 1840 times greater than electrons, so when they collide with the lattice atoms of the semiconductor they can dislodge or displace atoms from their lattice location causing them to take up interstitial positions within the crystal. This interaction results in a disruption or distortion of the local lattice structure. The site formally occupied by the atom in the lattice is called a vacancy, while the displaced atom is called an interstitial. Together they form a defect known as a vacancy-interstitial pair. Another possibility is the local distortion on the lattice where the bonds are not necessarily broken and the displaced atom remains near its originals location. This is known as a Frenkel Defect as shown in Figure 3.

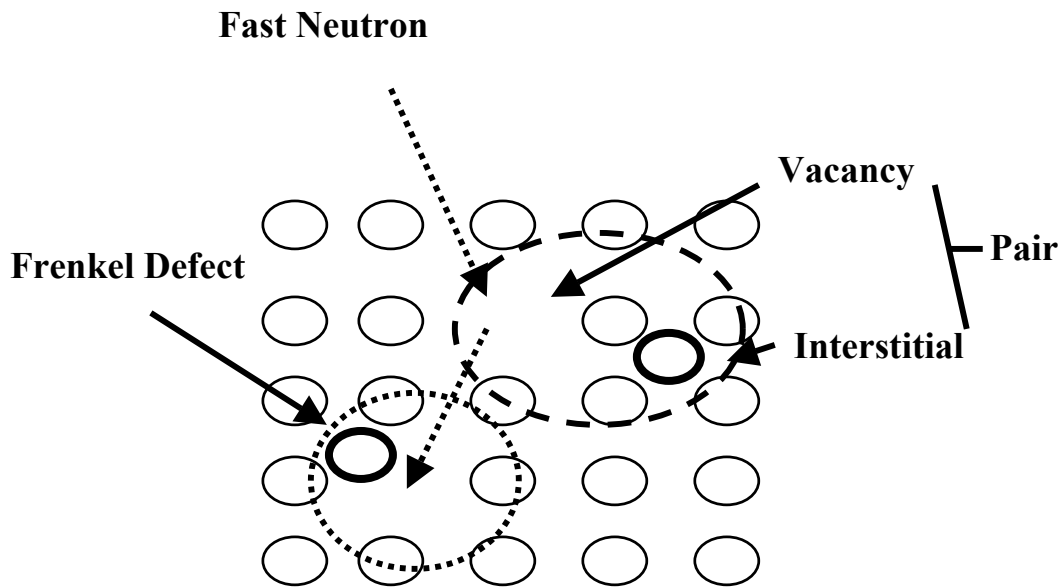


Figure 3: Formation of Defect Sites by Neutron Bombardment

If the energy of the incident neutron is sufficiently large it may impart enough energy to the displaced atom for it to displace additional atoms within the lattice, these atoms are called knock-on atoms. Highly energetic neutrons may cause many knock-on atoms to form and thus a single neutron can cause a cascade effect within the lattice causing defect clusters to form.

Eventually the displaced atoms lose their kinetic energy reaching thermal equilibrium within the lattice. Some atoms may move into a vacancy and recombine, while other atoms may interact with the dopant or other impurity atoms to produce stable defects. Electrically inactive defects do not constitute recombination or trapping centers and in small numbers may not affect the semiconductor's performance. However, mobile vacancies can combine with impurity atoms, donor atoms, or other vacancies present to produce room temperature stable defects. These defects are also called defect complexes

and can be effective recombination or trapping centers capable of significantly changing the electrical and optical properties of a device (Summers, IV-6).

Neutrons are also capable of producing ionization due to secondary effects. Neutrons can ionize through other processes such as: (a) neutron collisions that produce recoil atoms or ions, which in turn may ionize, (b) neutron collisions that excite atomic nuclei, which de-excite through gamma ray emission which can ionize, (c) neutron collisions where the neutron is absorbed by the target nucleus, which emits a charged particle (i.e. alpha particle), and (d) neutron induced fission of trace elements found in semiconductors such as uranium or thorium that can produce a heavy fission fragment (Messenger *et al*, 203). These ionization processes generally are not as devastating to long-term device performance as atomic dislocations but can cause significant problems if they become a dominant damage mechanism.

Since neutron damage varies as a function of neutron energy and the target material, it is common to discuss neutron exposure in terms of exposed fluence and not absorbed dose. It is also common to express neutron fluence in terms of a 1-MeV equivalent fluence (Northrup, 693). Designers do not usually care about absorbed dose, they simply want to know when, given a specified condition, a device will fail. The practice of only looking at the 1 MeV contribution of the fluence allows the comparison of damage to different semiconductor materials, independent of the neutron source. Gamma radiation can also be a potential problem but is generally much more penetrating and thus much less likely to cause damage in thin samples than incident neutrons.

III. Experiment

Experimental Procedure

This study consists of three main parts: 1) neutron irradiation of the target material, 2) fabrication of devices appropriate for analysis, and 3) analysis of the material using laboratory test techniques. The material being studied consists of four, research grade 4H-silicon carbide wafers, purchased from Cree Research Inc. (Cree, 2001). Table 2 lists the manufacturer's wafer properties and the intended method of analysis for each sample.

Table 2: Experimental Material Characteristics

Wafer #	Dopant	Epilayer Doping (N_D-N_A) (cm^{-2})	Wafer Thickness (μm)	Diameter (Inches)	Growth Orientation	Resistivity (Ohm-cm)	Planned Method of Analysis
1	N-type Nitrogen	1.2E17	377	2	7°50'	.021	PL/DLTS
2	P-type Aluminum	1.5E18	380	2	7°54'	4.3	PL/DLTS
3	N on P Nitrogen	1.2E17	362	2	7°49'	3.0	Hall
4	P on N Aluminum	1.3E18	360	2	7°52'	.019	Hall

The sample material was prepared as described in Appendix B and was irradiated in the manner listed in the Irradiation Test Plan (Appendix A). Following irradiation, two types of devices were fabricated: 1) ohmic van der Pauw contacts for Hall effect measurements and 2) Schottky diodes required for Deep Level Transient Spectroscopy (DLTS) measurements. PL samples were cleaned after irradiation but no further processing was required. Device fabrication and testing was conducted at the Air Force Institute of Technology, Wright-Patterson Air Force Base, Ohio. The irradiation work

was conducted at The Ohio State University Fission Research Reactor in Columbus, Ohio.

Neutron Irradiation

The irradiation dose to SiC was determined based on the fluence and flux calculations of the source. Once determined, a set of fluences was selected that would span the range from, no measurable effects, to the expected material breakdown point. Silicon-based devices may fail to perform properly at fluences of 10^{12} n/cm², but most manufacturing technologies are capable of producing devices capable of performing in fluences of 10^{14} or 10^{15} n/cm² (Northrop, 693). Previous studies indicate that SiC devices fail around 10^{17} n/cm². Using the Si baseline and noting the material properties of SiC, which suggest a higher neutron tolerance, fluences ranging from 10^{12} to 10^{18} n/cm² were selected for study in this project.

To ensure the accuracy of the intended fluence, the irradiation facility provided the neutron energy spectrum for its central irradiation facility as shown in Figure 4 (Ohio State, 2001). The neutron fluence for this source was well characterized for neutron energies from zero to 14 MeV and tabulated in 622 energy bins.

Accurate silicon carbide cross-section data was not readily available, therefore cross-section data for silicon and carbon was obtained from the Evaluated Nuclear Data Files (ENDF) and the spectrum was reconstructed to relate dose vs. energy and to construct cross-sections across energy bins corresponding to the neutron source (Chapman, 1998).

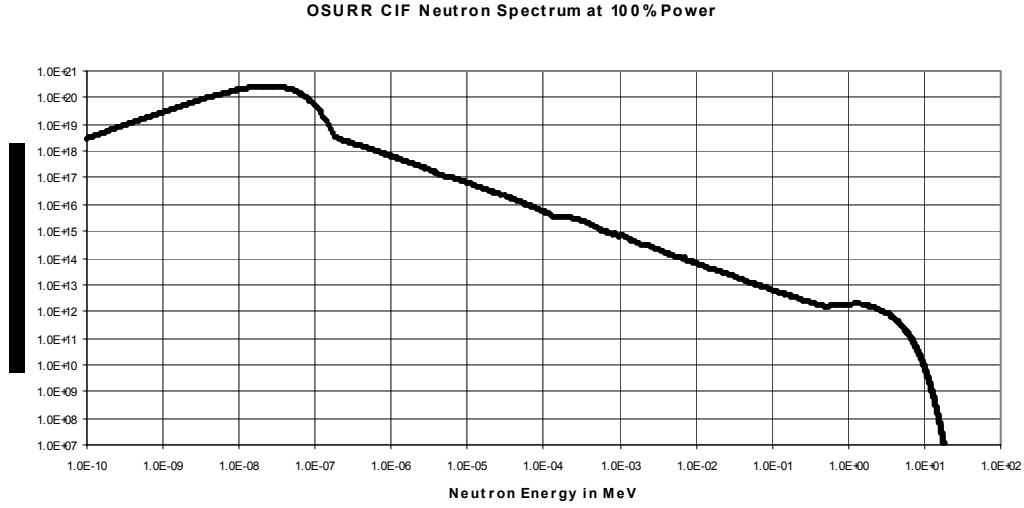


Figure 4: OSURR Reactor Fission Spectrum

In order to best normalize the spectrum to 1 MeV equivalent, it was necessary to “harden” the spectrum. To do this a thickness of cadmium was selected that would effectively reduce the thermal neutrons flux (1 eV or less) by 99.9 % so that their 1MeV contribution was negligible. This can be important when considering the average energy needed to displace a SiC atom from the lattice, which is approximately 41 eV (Summers, IV-7). Based upon calculations contained in Appendix A, a 4-millimeter cadmium absorber was selected. Next, a 1 MeV fluence rate (flux) was calculated using Equation 1 (Turner, 368).

$$\Psi(1\text{MeV}) = \frac{\sum_{E=1}^{E_{\text{max}}} \Psi(e) \cdot \left(\frac{\mu(e)}{\rho} \right) \cdot E}{\left[\left(\frac{\mu(1\cdot\text{MeV})}{\rho} \right) \cdot (1\cdot\text{MeV}) \right]} \quad (1)$$

Where:

$\Psi(1\text{MeV})$ = 1 MeV Equivalent Flux

$\Psi(e)$ = Fluence at a Particular Energy Group

E = The Average Value of the Current Energy Bin

E_{max} = The Last Energy Group (Highest Energy)
 ρ = The Material Density
 $\mu(e)$ = The Macroscopic Cross Section for a Particular Energy Group
(note: the numerator is also the Dose Rate)

Using the source full-power flux and the target fluences, the time needed to achieve the desired fluence was calculated. Because the OSURR neutron fluence retains its energy distribution over a majority of the power range, the full power time can be used to determine total fluence, and the reactor power can be adjusted to obtain a lower fluence. In this way all irradiations occur over the same time, reducing the chance that thermal annealing will differ significantly from one group to another. Heat buildup within the samples is minimal with the greatest heat source being the cadmium shield, which could reach temperatures as high as 400 K during a sample run. This is small as compared to defect annealing temperatures of 900 to 1300 K (Scott, VI-35).

Device Fabrication

All useful semiconductor electronics require conductive signal paths in and out of each device (Neudeck, 22). While SiC itself is theoretically capable of operation under extreme electrical and thermal conditions, it is useless unless contacts can be made that will withstand the same conditions. For the purpose of this study, quality, repeatable contact formation and processing is essential and the subject of a great amount of effort. Two of the chosen analysis techniques, Hall, and DLTS, required the formation of quality contacts, while the third, PL, required only clean material. Contacts were required to withstand sustained temperatures of 100 – 700 K and were applied post-irradiation to avoid neutron activation.

Ohmic contacts were formed to carry electrical current into and out of the semiconductor, ideally with insignificant parasitic resistance. The material, the dopant type, and dopant level all heavily impact the choices for this contact. After some exploration and trial it was determined that the best ohmic contacts could be formed with nickel as the n-type ohmic metal and Al/Ti as the p-type metal. These required a contact anneal process in order to form ohmic contacts, with very low parasitic resistance.

Rectifying contacts serve another purpose and are the key to forming the capacitance bearing Schottky diodes needed for DLTS measurements. Nearly all un-annealed metal contacts to lightly doped 4H-SiC are rectifying, however Ti was chosen as using it produced devices with a low reverse bias leakage current.

Appendix B contains the sample preparation, contact formation recipe cards that were developed and used during the course of this study, and a list of the chemicals used in processing. Table 3 lists the key fabrication steps required for each group of samples.

Table 3: Required Preparation of Samples

Sample Type	Initial Clean & Cut	Post Irradiation Clean	Acid Etch	Ohmic Backside Contacts	Ohmic van der Pauw Contacts	Contact Anneal	Rectifying Schottky Contacts
(N & P-Type) PL	X	X					
N-Type Hall	X	X	5 Min		2000 Å Nickel	5 Min @ 1100°	
P-Type Hall	X	X	5 Min		200 Å Ti + 1800 Å Aluminum	5 Min @ 1100°	
N-Type DLTS	X	X	5 Min	2000 Å Nickel		5 Min @ 1100°	2000 Å Titanium
P-Type DLTS	X	X	5 Min	200 Å Ti + 1800 Å Aluminum		2 Min @ 900°	2000 Å Titanium

Photoluminescence requires no contact formation, therefore samples destined for PL only required cleaning steps. DLTS required the formation of Schottky diodes. Figure 5 is the configuration for a two-sided Schottky diode (Crockett, 2002). The Schottky diodes used in this study consist of an ohmic backside layer and a grouping of 500 Å diameter, rectifying contacts.

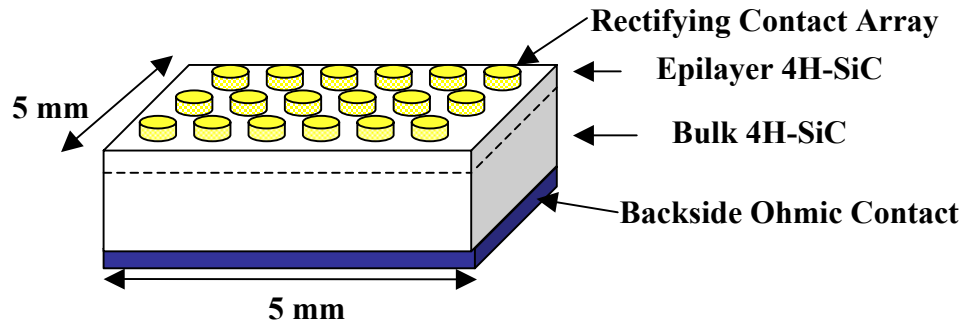


Figure 5: Two-Sided Schottky Diode for DLTS Experiment

Hall Effect measurements require a somewhat simpler device consisting of four, 500 Å diameter, ohmic contacts spread apart as far as is reasonable on the front side of the sample as shown in Figure 6. This configuration is commonly called a van der Pauw configuration (Schroder, 14).

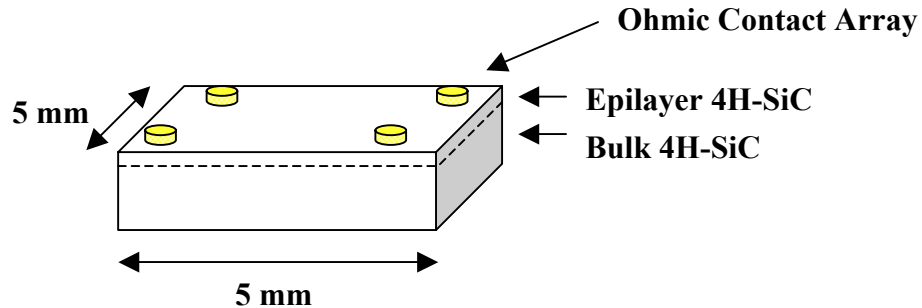


Figure 6: van der Pauw Contact for Hall Effect Experiment

Sample Analysis Techniques

Based upon time, resources, and the desired properties to be studied it was decided to utilize three primary laboratory techniques in this project. Additional laboratory observations and measurements were taken as a routine part of the experiment and are noted in Chapter IV.

Photoluminescence (PL)

Photoluminescence (PL), also known as fluorometry, provides a nondestructive technique for the determination of impurities in semiconductors such as SiC. It is particularly suited for detection of shallow-level impurities, but can be applied to some deep-level impurities, provided their recombination is radiative (Schroder, 109). The technique involves shining a high intensity light source, frequently a laser, with energy greater than the semiconductor bandgap ($h\nu > E_g$), onto a materials surface, generating electron-hole pairs (eh) that recombine by one of several mechanisms. Photons are emitted for radiative recombination but not emitted for nonradiative recombination. For quality PL output, the majority of the recombination processes should be radiative (Schoder, 623).

Since the sample is excited optically and emitted photons are collected to take a measurement, electrical contacts and junctions are unnecessary and highly resistive materials like 4H-SiC that have been exposed to a high neutron flux pose no practical difficulty for measurement. Figure 7 shows the typical output of a photoluminescence measurement.

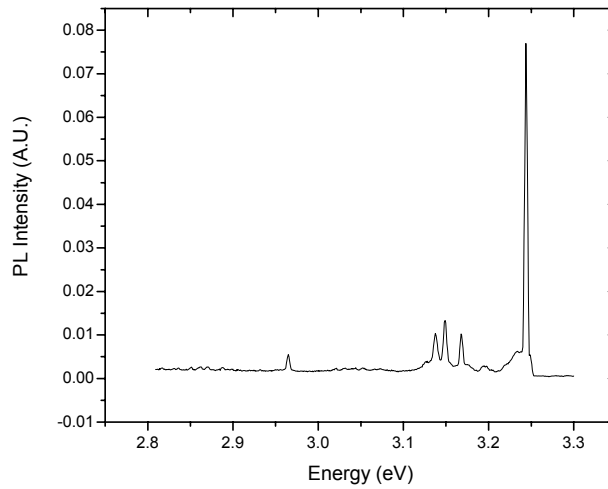


Figure 7: PL Spectrum from an Unirradiated n-type 4H-SiC Sample

Low temperature measurements, less than 10 K, are necessary to obtain the fullest spectroscopic information by minimizing thermally active nonradiative processes and thermal line broadening which may dominate.

The emitted photon energy depends upon the specific recombination process. Figure 8 depicts five of the most commonly observed PL transitions. Band-to-band recombination dominates at room temperature, however, it is rarely observed at low temperatures in materials with small effective masses (due to the large electron orbital radii) (Figure 8a). A more common transition is excitonic recombination (Figure 8b). When a photon creates an electron-hole pair (ehp), the electron and hole may remain bound together in an excited state called a free exciton. In order to conserve momentum its energy must be slightly less than the bandgap energy required when creating a separated ehp. Since they move together neither photoconductivity or current is created, but when they recombine photon emission may occur. When a free hole combines with a

neutral donor they may form a positively charged exciton or bound exciton (Figure 8c). The electron bound to the donor travels in a wide orbit about the donor. Similarly electrons combining with neutral acceptors also form bound excitons. In an indirect bandgap semiconductor such as SiC this exciton recombination process must be assisted by the emission of a phonon in order to conserve momentum in the transition. Another common recombination event can occur when a hole (electron) combines with a neutral acceptor (donor) (Figure 8d). Lastly, an electron on a neutral donor can recombine with a hole on a neutral acceptor causing donor-acceptor recombination (Figure 8e).

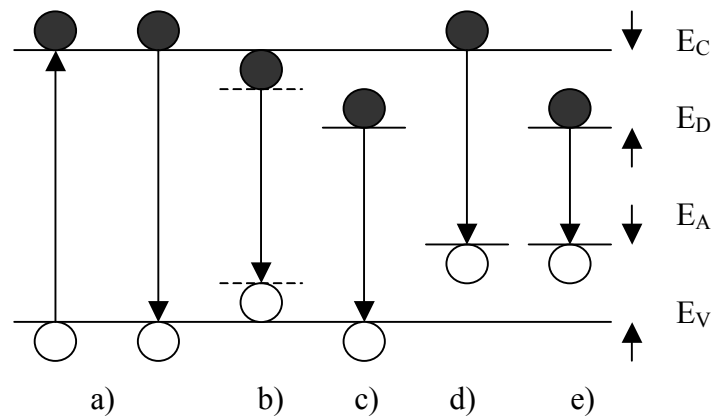


Figure 8: Radiative Transitions Observed with PL

(a) Band to band recombination. (b) Free exciton recombination. (c) Bound exciton recombination. (d) Free electron-acceptor recombination (or free hole-donor) (e) Donor-acceptor recombination (Schroder, 624)

The output of a photoluminescence measurement can be expressed in terms of energy (eV) such as shown in Figure 7 or in terms of emission wavelength in angstroms as related by Planck's constant using Equation 44.

$$h\nu(\text{eV}) = \frac{12400}{\lambda(\text{angstroms})} \quad (44)$$

The minimum equipment needed to perform PL is modest: an optical source with an energy greater than the material bandgap and an optical power meter or spectrophotometer, although practical systems are somewhat more robust. A typical PL setup is shown in Figure 9 (Gfroerer, 2).

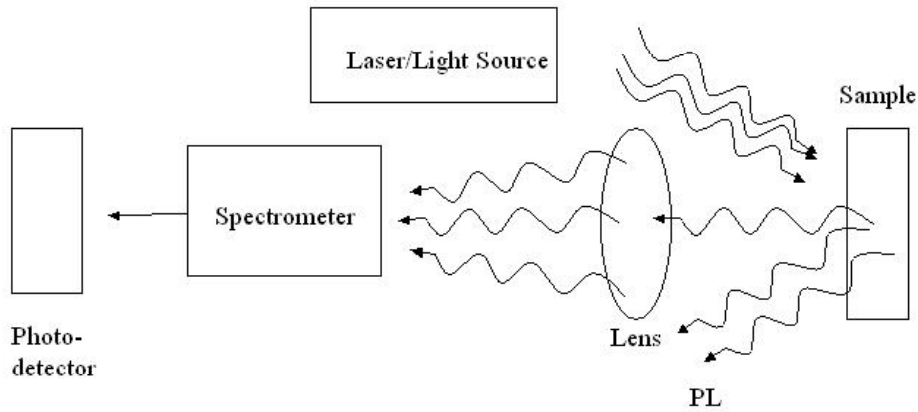


Figure 9: Typical Photoluminescence Experimental Setup

The system used for this experiment is set up as shown and consists of: a Spectra Physics 275 nm argon laser, operated at 0.6 watts; a Lake Shore 330 Temp Controller; SPEX 750M Spectrometer; and a Products of Research INC. nitrogen cooled GaAs photo-multiplier tube.

Constant Voltage Deep Level Transient Spectroscopy (CV-DLTS)

DLTS was developed in 1974 by D.V. Lang who built upon the groundbreaking work of C.T. Sah done in 1970 (UM, 2001). Before this technique, deep states were detected using detrapping techniques, such as thermally stimulated current (TSC) and capacitance (TSCAP), or by directly recording the capacitance or current transients as a

function of time (Scott, IV-4). Lang introduced the rate window concept to deep level impurity characterization in a technique referred to as the double boxcar approach or deep level transient spectroscopy (DLTS).

Since 1974, over 30 variations of DLTS have subsequently been developed for application in a variety of specific conditions. The fundamental concept in all these variations is the transient behavior of the filling and emptying of the defect sites by thermal or optical stimulation. Of these 30 variations, the three that lend themselves nicely to applications involving semiconductor devices are most commonly used. They are constant-voltage DLTS (CV-DLTS), constant-capacitance DLTS (CC-DLTS), and double-correlated DLTS (DDLTS). Each of these methods measures the transient capacitance or voltage with the device sample in reverse bias (depletion). There are several advantages for using these depletion region techniques:

- a) The charge transients on deep states in the depletion region can be monitored by measuring the depletion capacitance or the device current.
- b) The measurements are very sensitive. The ratio of values can be as low as $N_t/(N_d-N_a) = 10^{-5}$, where N_t is the trap concentration, N_a is the acceptor concentration, and N_d is the donor concentration.
- c) Trap response is determined by more than one process, so in depletion the capture process can be suppressed.
- d) Trap filling by majority carriers can be introduced by lowering the reverse bias and re-admitting electrons to the observation region.
- e) By controlling the bias during trap filling and emptying, the spatial extent of the observation region can be controlled and depth profiling is possible.

f) By controlling the bias during trap filling and emptying, the electric field strength in the depletion region can be controlled which allows characterization of the trap's charge state.

In DLTS, the material being studied is typically fabricated into a junction device, such as a Schottky or p-n junction diode. For the p-n diode, one side is heavily doped relative to the side being studied. This allows for a depletion region to be formed mainly in the lightly doped side with an applied reverse bias. Uniform doping is preferred as this allows the depletion depth to vary proportionally to the square root of the applied voltage. This device design is known as a one-sided abrupt junction. A Schottky diode differs from a p-n diode by the replacement of the higher doped side with a rectifying metal contact. All calculations associated with DLTS apply to both types of diodes.

To date, there is no satisfactory theory for calculating the observed electronic properties of deep states; therefore indirect correlations with device processing are used to assign these levels to specific centers. DLTS is thus used to measure activation energy, effective capture cross-section, and relative concentration, and also to identify the most likely constituents forming the specific deep state.

Double-correlated deep level transient spectroscopy (DDLTS) is used to probe the depletion region. Probing the depletion region permits the development of a concentration profile of the deep level defects and permits measuring the effect of the electric field on the trapping kinetics of the deep level defects. Constant capacitance deep level transient spectroscopy (CC-DLTS) is used to measure interface state densities, provided that the deep level density is no more than an order of magnitude lower than the dopant density. Deep state concentrations and properties are important for; 1) overall

quality characterization, 2) understanding speed of response limits, and 3) establishing the influence of the defects and impurity centers in carrier recombination.

Constant Voltage Deep Level Transient Spectroscopy (CV-DLTS), which was used for this experiment, consists of the application of a constant reverse bias voltage across a Schottky diode, which creates a depletion region and depletes the majority carriers. A slight forward bias or removal of the negative bias is then applied as a step-signal to create a filling pulse and fill the trap centers in the material as the Fermi level is raised above the trap energy level. Once the traps are filled the depletion is reestablished and a series of measurements are then taken which measure the detrapping time of the occupied sites. These traps then proceed to thermally emit the trapped carriers until they are empty. The nonzero electric field in the depletion region sweeps the emitted carriers away before they can be recaptured by the traps (Scott, IV-7).

The resulting capacitance vs. time curve is then analyzed using the rate window concept of deep-level impurity characterization. If the capacitance vs. temperature ($C - t$) curve from a transient capacitance experiment is measured so that a selected decay rate produces a maximum output, then a signal whose decay time changes monotonically with time reaches a peak when a rate passes through the rate window of a boxcar averager or the frequency of a lock-in amplifier. A repetitive $C - t$ transient can be observed through such a rate window when the decay time constant is varied, by changing the sample temperature. Using this technique may cause a peak to appear in the difference capacitance versus temperature plot at the location of a trap site (Schroder, 290). Such a plot is a DLTS spectrum as shown in Figure 10. This technique is used to extract a

maximum in a decaying waveform and is a function of capacitance, current, charge transients, and trap parameters.

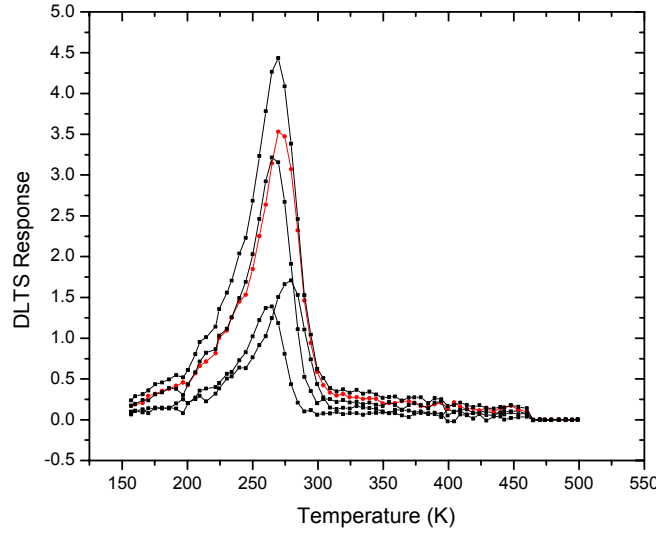


Figure 10: Measured DLTS Spectrum of Irradiated 4H-SiC

The capacitance decay waveform is typically corrupted with noise, so many measurements are taken and averaged. To accomplish this, DLTS uses a correlation technique, which is a signal processing method with an input signal multiplied by a reference signal, a weighting function, and the product filtered (averaged) by a linear amplifier. This allows the extraction of a ΔC unique to a specific sampling period.

In the Boxcar Method of DLTS, the $C - t$ waveform is sampled (or gated) at times $t = t_1$ and $t = t_2$ and the capacitance at t_2 is subtracted from the capacitance at t_1 . This difference signal ($C_{t2} - C_{t1}$), is the standard output of a double boxcar instrument. The temperature is slowly changed while the device is repetitively pulsed. There is no difference between the capacitance at the two sampling times (C_{t2} , C_{t1}) for very slow or

for very fast transients, corresponding to low and high temperature. However, a difference signal is generated when the time constant is on the order of the gate separation $t_2 - t_1$, and the capacitance difference passes through a maximum as a function of temperature as shown in Figure 11 (Crockett, 2002).

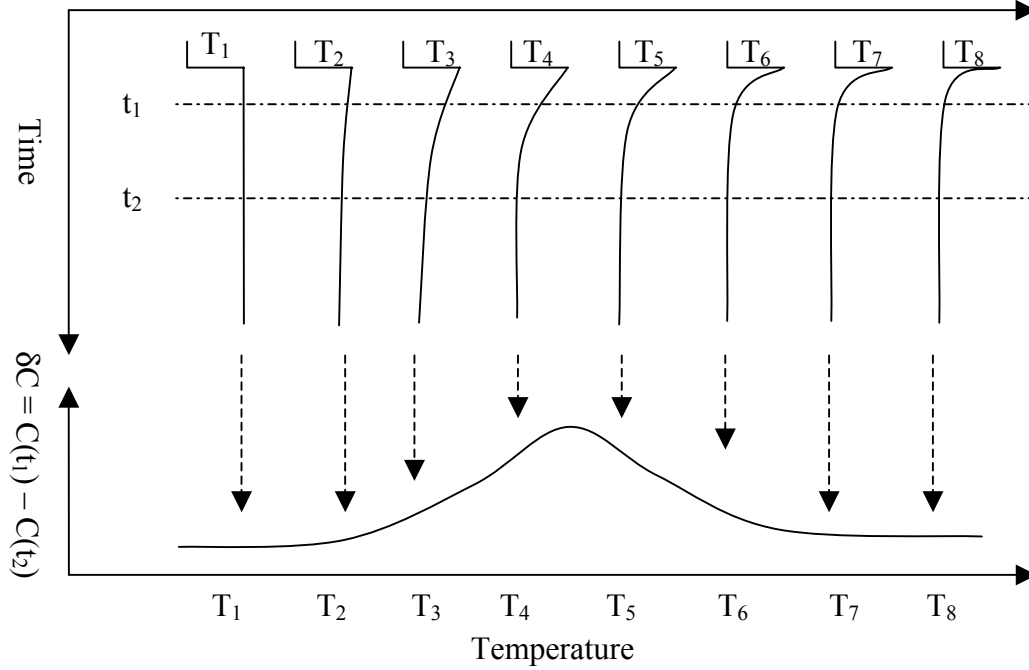


Figure 11: Capacitance Transients at Various Temperatures

Also of interest is the time constant for majority carrier emission as computed using Equation 2.

$$\tau_{e(\max)} = \frac{t_2 - t_1}{\ln\left(\frac{t_2}{t_1}\right)} \quad (2)$$

where

$\tau_{e(\max)}$ = time constant for majority carrier emission
 t_1 = time of first measurement
 t_2 = time of second measurement

By generating a series of $C - t$ curves at different temperatures for a given gate setting t_1 and t_2 , one value of τ_e corresponding to a particular temperature is generated, giving one datum on a $\ln(\tau_e T^2)$ versus $1/T$ plot. The measurement sequence is then repeated for another t_1 and t_2 gate setting for another point. In this manner a series of points are obtained to generate an Arrhenius plot as shown in Figure 12.

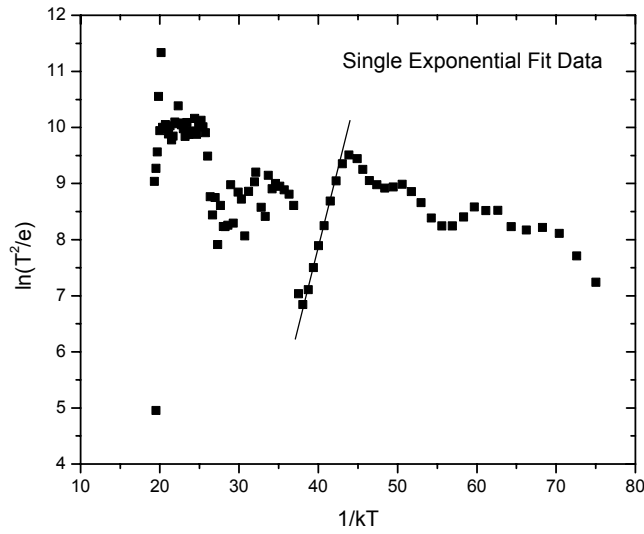


Figure 12: Measured Arrhenius Plot from Irradiated 4H-SiC

Data plotted in this manner is of no value unless a positive sloped trend line can fit to the data. The slope of the line (lines), the relative location of the line, and other collected data allow the user to extract three critical details about a potential defect site, activation energy (E_t), capture cross-section (σ_t), and density (N_t).

Typical DLTS experiments contain the following hardware, as shown in Figure 13: capacitance bridge with pulse couple circuit; double pulse generator; cryostat unit;

computer (for controlling measurements and storing results); and a temperature controller (TUB, 2001).

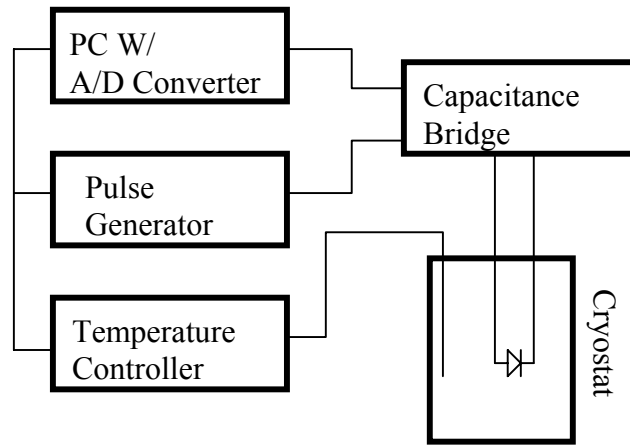


Figure 13: Typical DLTS Setup

The system used consists of a PC w/ controller card, LeCroy 9210 Pulse Generator, LeCroy 9410 Oscilloscope (used only to verify pulse output), Lake Shore 330 Temperature Controller, Alcatel Drytel 31 vacuum pump, CTI-Cryogenetics Model 22 Cryodyne Refrigerator, CTI-Cryogenetics Model 8200 Compressor, and a Sula Technologies Deep Level Spectrometer. Data analysis was performed using the Arrhenius6 software package with a user interface shown in Figure 14.

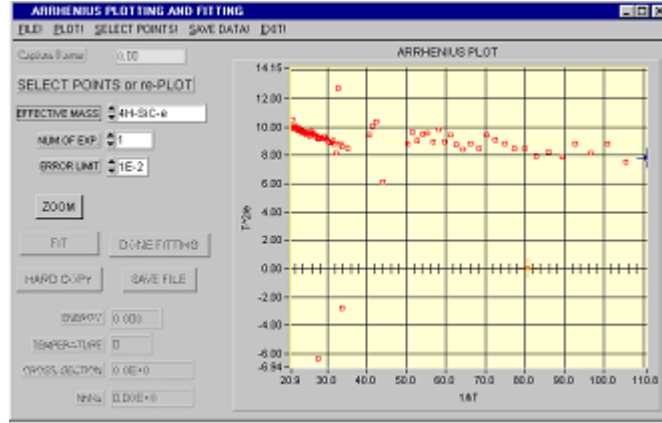


Figure 14: Arrhenius Plot Analysis Software Interface

Hall Effect Measurements (HALL)

The Hall effect measurement was first used in 1879 when Edwin H. Hall discovered that a small transverse voltage appeared across a current carrying thin metal strip in an applied magnetic field. He used this to measure the resistivity of materials. It was not until later that scientists realized that resistivity was not a fundamental property of material either, as different materials may have the same resistivity. This is especially true of semiconductors, so the definitions of carrier density, n , and mobility, μ , were defined, making the Hall effect measurement increasingly valuable. The technique has since been developed into a mature and practical tool that is routinely used for test electrical properties and quality of almost all semiconductor materials (NIST, 2001).

The basic principle of the Hall effect is its use of the Lorentz Force as shown in Equation 5. When an electron moves along a direction perpendicular to an applied magnetic field, it experiences a force acting normal to both directions and moves in response to this force and the force effected by the internal electric field.

$$F = q(\mathcal{E} + \mathbf{v} \times \mathbf{B}) \quad (5)$$

where

$q = 1.6 \times 10^{-19}$ coulombs

B = magnetic field

ε = Voltage

v = drift velocity

Figure 15 is an illustration of the Hall effect in a p-type sample. In this sample the carriers are mostly holes (Schroder, 511).

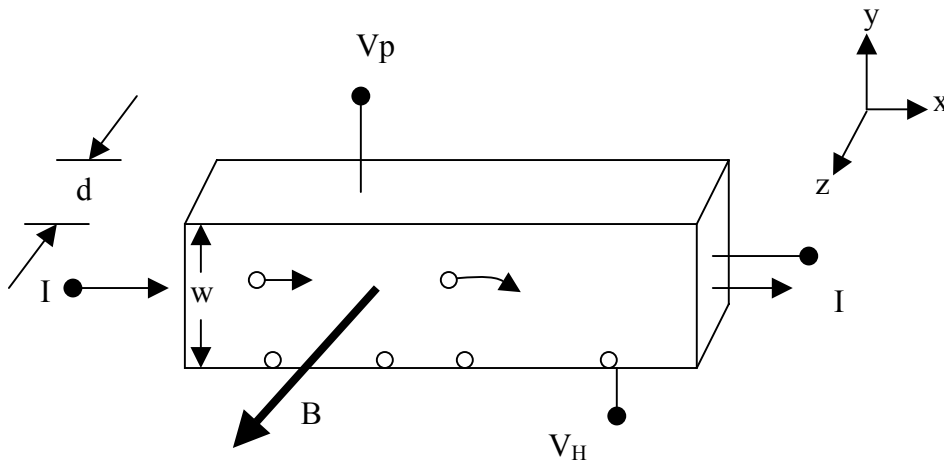


Figure 15: Illustration of Hall Effect in a p-type Sample

A constant current is applied along the x direction flowing from left to right in the presence of a magnetic field in the z direction. Holes subject to the Lorentz force initially drift away from the current flow toward the negative y-axis, resulting in an excess number of holes on that side of the sample. The interaction of the Lorentz force with the Hall electric field creates a transverse voltage, known as the Hall Voltage given by Equation 6.

$$V_H = \frac{I \cdot B}{q \cdot n \cdot d} \quad (6)$$

Where:

I = current
 B = magnetic field
 $q = 1.602 \times 10^{-19} \text{ C}$
 n = bulk density
 d = sample thickness

By using layer or sheet density ($n_s = n \times d$) and rearranging the terms, we obtain Equation 7, which defines the sheet density of majority charge carriers.

$$n_s = \frac{I \cdot B}{q \cdot |V_H|} \quad (7)$$

By measuring the Hall Voltage and knowing the values of I, B, and q, we can obtain the carrier density.

Depending upon device configuration the value for the Hall Voltage will be either positive or negative. The sign of the voltage tells us whether the semiconductor is p- or n-type.

The computation of the mobility, μ , is dependent upon the computation of the sheet resistance R_s . The sheet resistivity is typically computed using the van der Pauw resistivity measurement technique. Since mobility and sheet density are components of the sheet resistivity it is possible to solve directly for mobility once the other values are known as in Equation 8.

$$\mu = \frac{|V_H|}{R_s \cdot I \cdot B} = \frac{1}{q \cdot n_s \cdot R_s} \quad (8)$$

Typical Hall systems contain a magnet, current source, high input voltmeter, sample holder (located in the center of a uniform magnetic field), and sample temperature

probe as shown in Figure 16. More elaborate PC-controlled automated systems are simple to construct based upon the basic components.

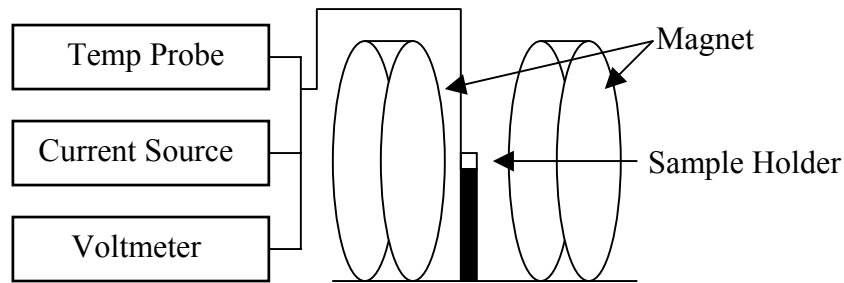


Figure 16: Typical Hall Set Up

The AFIT System as used consists of a Walker Scientific INC magnet and gauss meter w/ power supply current controller, Alcatel Drytel 31 vacuum pump, RMC Cryosystems refrigerator, Lake Shore DRC-91CA temperature controller, Keithley 220 programmable current source, Keithley 196 system DMM, Keithley 706 scanner, Keithley 617 programmable electrometer, and Keithley quad electrometer buffer amplifier.

IV. Results

Observed results were collected over a period of 4 months. Observations are grouped into n- and p-type silicon carbide. Although PL, DLTS, and Hall effect are the primary evaluation tools, additional observations were made when deemed necessary. In general, the n-type samples proved more revealing because n-type devices were easier to fabricate and more defect structure was observed in the n-type material. This may be attributed to the difference in dopant for the materials. The n-type uses a nitrogen dopant while the p-type uses an aluminum dopant. Since intrinsic SiC is slightly n-type, it is less compensated than p-type SiC for the same net doping concentration. Therefore, fewer lattice displacements are likely to occur during the implantation process.

N- Type Silicon Carbide

Observations of n-type SiC are recorded based upon two wafers of nitrogen-doped silicon carbide. The first wafer has an epilayer doping of $N_D - N_A = 1.2 \times 10^{17} \text{ cm}^{-3}$ and provides samples for both PL and DLTS analysis. The second wafer has a thin nitrogen doped epilayer of $N_D - N_A = 1.2 \times 10^{17} \text{ cm}^{-3}$ grown on a p-type substrate. This wafer provides the thin electrically isolated channel required for quality Hall effect measurements.

n-type Photoluminescence Results

The n-type 4H-SiC proved to be a quality subject for PL analysis in that a strong emission response was obtained. Figure 17 is representative of the spectrum obtained using a typical non-irradiated sample, and dominated by a zero phonon line (ZPL) (recombination without phonon emission) occurring at 3.244 eV. The occurrence of this

feature and its location have been widely reported, and is commonly attributed to its relationship with the recombination of excitons bound at neutral nitrogen donors (nitrogen that has replaced the carbon atom, N_C^0) in the cubic sites within the crystal (Harris, 29). However, as stated earlier, the silicon carbide lattice is made up of two types of sites, quasi-cubic and hexagonal, causing the ZPLs to be present in pairs.

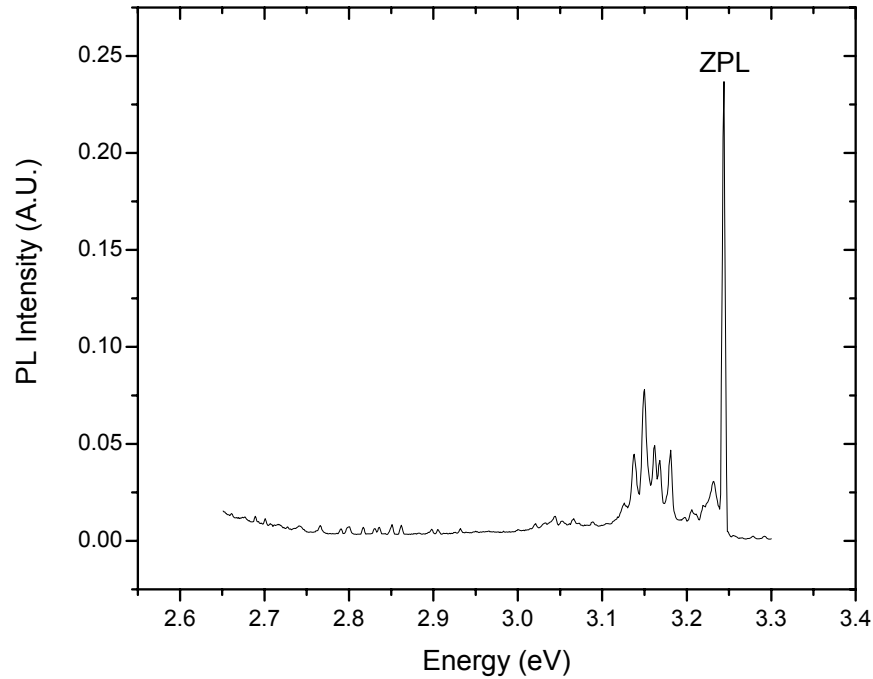


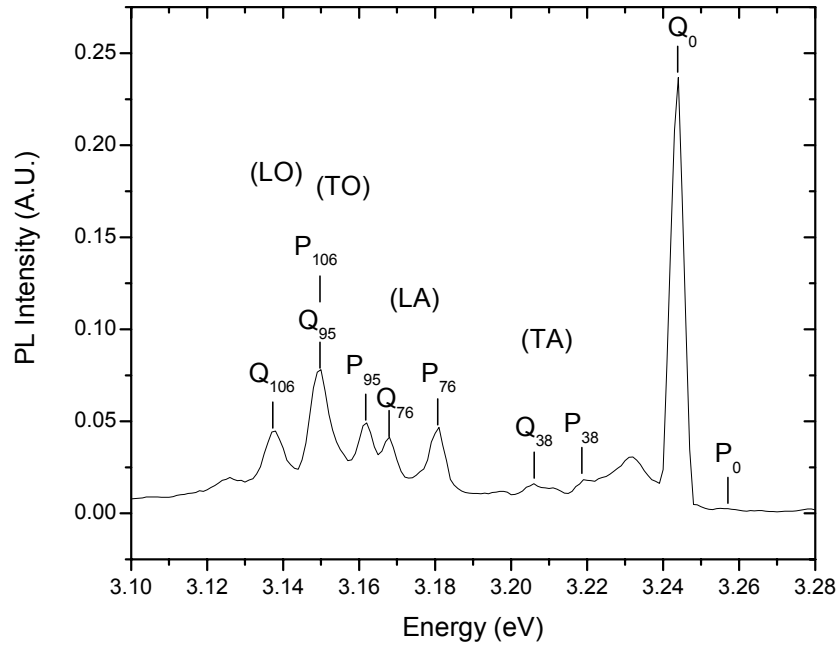
Figure 17: PL Spectrum for Un-irradiated n-type 4H Silicon Carbide

This study focused on the ZPLs and their associated phonon replicas nearest the bandgap of 3.24 eV. This was the region of highest spectral resolution. Defect sites deeper than ~ 2.7 eV were effectively masked by a strong broad luminance peak. Table 4, is a list of expected zero phonon line replica locations (Harris, 30).

Table 4: Reported Energy of ZPL Phonon Replicas for 4H-SiC

Phonon Branch	4H-SiC (meV)
TA	46
LA	79
TO	94
LO	103

Figure 18 lists the location of the first ten ZPLs and replicas as measured in n-type SiC. Additional notation is required because of the separate phonon replicas. The notation used is; 1) transverse acoustic (TA), 2) longitudinal acoustic (LA), 3) transverse optical (TO), and 4) longitudinal optical phonons (LO). This is accurate for the cubic polytype, and typically is used to represent both the cubic and hexagon sites (Scott, VI-80). It should also be noted that these replica peaks occupy nearly the same energy range in other SiC polytypes, but their spectral intensity varies.

**Figure 18: Observed PL Peaks in n-type 4H SiC**

The spectral effect of neutron irradiation on the samples is shown in Figure 19, where the samples shown were exposed to the listed fluence of 1 MeV neutrons. Most clearly shown is the reduction of the ZPLs luminescence as a function of irradiation. Since the ZPLs represent the recombination without phonon emission sites, it appears that the dislocation damage caused by the neutron fluence quickly suppresses this type of emission. Three reasons may explain this response. First the neutron cross-section for nitrogen is almost twice that for carbon or silicon in both the thermal and epi-thermal (< 1 MeV) range causing proportionally greater nitrogen displacement (ENDF). Second, the bond strength of the carbon-site bound nitrogen donor is less than the natural carbon atom (Summers, IV-7). Third, the increasing opacity of the material may affect photon emission at these wavelengths.

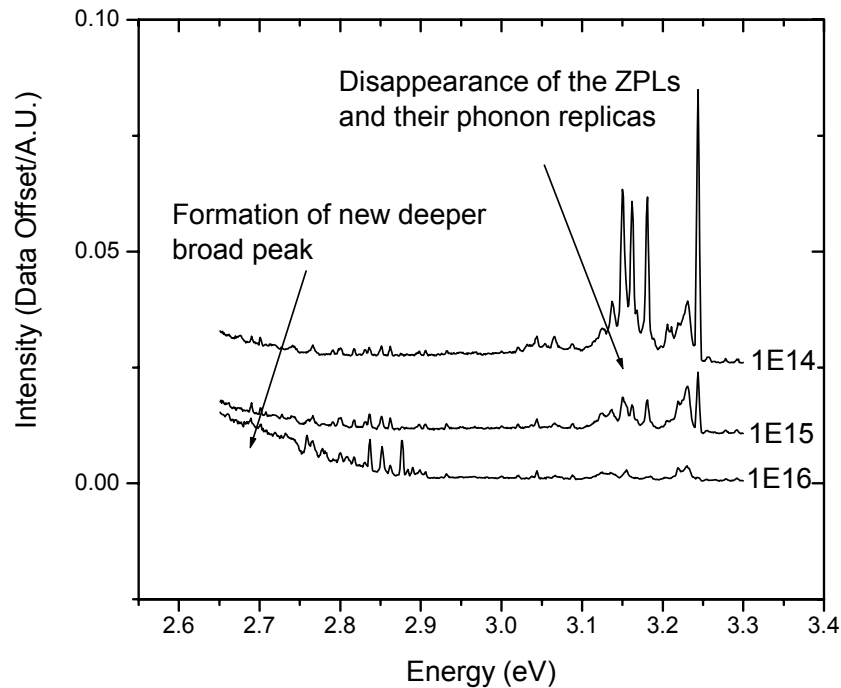


Figure 19: PL Response of n-type SiC to various Irradiation Levels

As irradiation fluence increases, the magnitudes of vacancy-interstitial pairs and Frenkel defects grow. The intensities of the ZPL phonon replica luminescence tend to be suppressed (or not occur in the first place) until the material fails to provide any measurable emission data. This occurs at a total neutron fluence of $1\text{E}16\text{ n/cm}^2$. This closely matches the electrical results as measured by the other means in this experiment and the results of other authors such as McLean *et al* (McLean, 1994). Another noticeable effect of increased neutron fluence was the formation of a deeper broad peak ($\sim 2.5\text{ eV}$) in the n-type 4H-SiC. This formation may be attributed to other defect complexes being formed as dislocation sites increase.

Also noted during the experiment was the sensitivity of PL peak intensities to input laser intensity. The Q_0 site (cubic-related) was the most sensitive peak to laser power. Therefore, great care was taken to ensure a common laser input intensity was maintained for each sample run. Temperature also had the potential to play an important role in spectral response, so care was taken to ensure all data was collected with sample temperature kept between 4 and 8 K to minimize thermal noise.

n-type DLTS Results

DLTS measurements were made using a wafer with an epilayer doping of $\text{N}_\text{D}-\text{N}_\text{A} = 1.2\text{E}17\text{ cm}^{-3}$. Measurements were conducted from 100 to 700 K using a computer controlled and triggered deep level transient spectrometer. Computer control provides an automated step approach to collect and record isothermal capacitance transients (Scott, VI-12). Post-test analysis was done using a software assisted, graphical curve fitting of the various rate window curves. Figure 20 shows the five rate window plots measured from a sample damaged with a $1\text{E}16\text{ n/cm}^2$ 1 MeV neutrons.

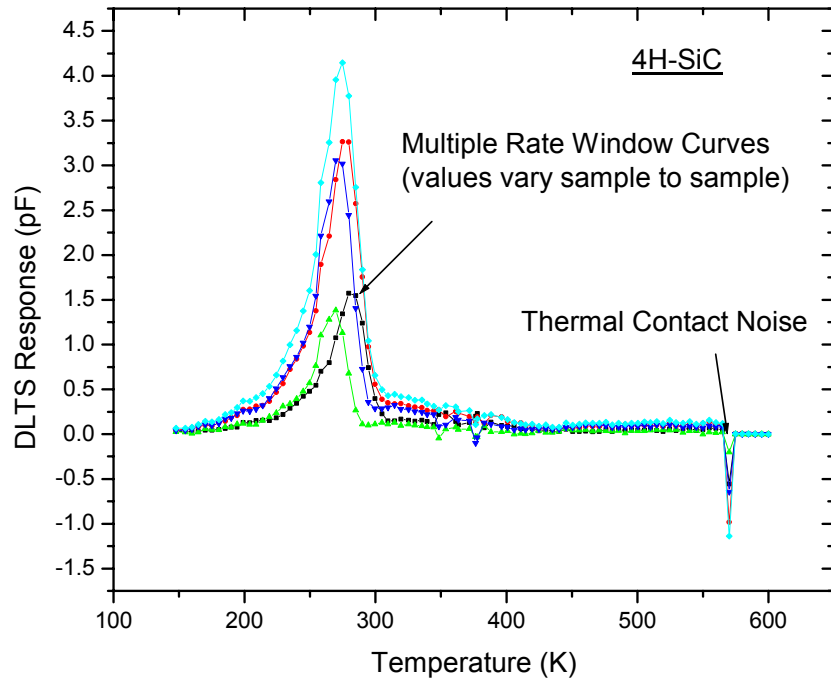


Figure 20: DLTS Rate Window Response of Damaged n-type SiC

The various curves represent varying rate windows and the capacitance response measured utilizing each of them. Samples that yield no measurable DLTS response curve yield no useful trap site information. The DLTS response data is then analyzed with the Arrhenius plot. Figure 21 is an example of the single exponential fit used to locate the 305 K trap in a $1\text{E}16 \text{ n/cm}^2$ neutron fluence sample.

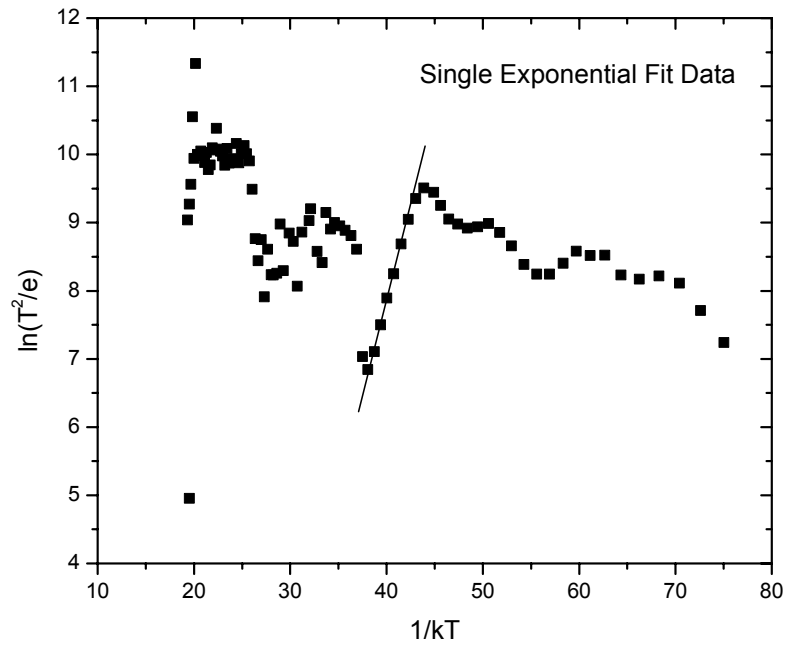


Figure 21: Arrhenius Plot Depiction of one Trap Site

The Arrhenius 6 software package was used to graphically fit and evaluate the Arrhenius plot data resulting in the observed defect data listed in Table 5.

Table 5: n-type 4H-SiC DLTS Results

1 MeV Neutron Fluence (n/cm²)	Temp of Peak (K)	Trap Energy (meV)	Capture Cross-section (cm²)	Trap Concentration (cm⁻³)	Exponential Used in Fit	Error Limit
1e16	305	492	2.4e-16	2.06e16	1	1e-4
1e16	310	693	1.0e-12	1.91e16	2	1e-4
1e16	482	265	1.3e-16	1.73e16	2	1e-3
1e16	255	520	1.2e-15	1.69e16	2	1e-4
5e15	290	435	1.8e-17	5.93e15	2	1e-3
5e15	255	550	2.9e-15	4.01e15	2	1e-4
5e15	305	473	1.0e-16	6.56e15	1	1e-4
1e15	300	515	7.1e-16	1.30e15	1	1e-3
1e15	295	736	7.1e-12	1.37e15	2	1e-3
1e15	273	753	1.9e-11	1.13e15	2	1e-3
1e15	311	458	1.1e-16	8.83e14	1	1e-3

Some data has been omitted based upon low cross sections that represent poor fitting in the Arrhenius plot. Multiple observances of a site at different irradiation levels are reported to show the relationship of a site to the neutron exposure of the sample. Table 4 shows that trap concentrations do increase as a function of increased exposed fluence. It also shows the emergence of a dual defect site at temperatures of 295 to 310 K, which is the same site shown in the DLTS response plot of Figure 20. We believe this grouping represents a single defect cluster that may dominate electrical performance at room temperature. This result is loosely correlated by observations of room temperature Hall effect. It may also be possible that other lower concentration sites are being formed in the higher irradiated samples, however, their observation is being masked by the leakage currents in those samples. Samples with irradiation levels above $1\text{E}16 \text{ n/cm}^2$ 1MeV neutrons were unable to be studied using this technique, as the Schottky leakage current exceeded $50 \mu\text{A}$ at a bias of -1.0 volt , which is needed to complete the sample measurement. Samples irradiated below $1\text{E}15 \text{ n/cm}^2$ resulted in good quality devices but failed to yield the existence of any deep level traps. The failure to detect sites in samples below $1\text{E}15 \text{ n/cm}^2$ is attributed to the detection limit of the test apparatus. The detection equipment has the ability to detect traps with concentrations around $1\text{E}-5 \text{ cm}^{-3}$ below the dopant, for that reason DLTS is normally performed on sample with dopants $\sim 1\text{E}15 \text{ cm}^{-3}$. As stated earlier, the samples used in this study were doped to $1.2\text{E}17 \text{ cm}^{-3}$ in order to facilitate the formation of quality contacts. This high dopant level may be masking defect structure in as grown and slightly irradiated samples.

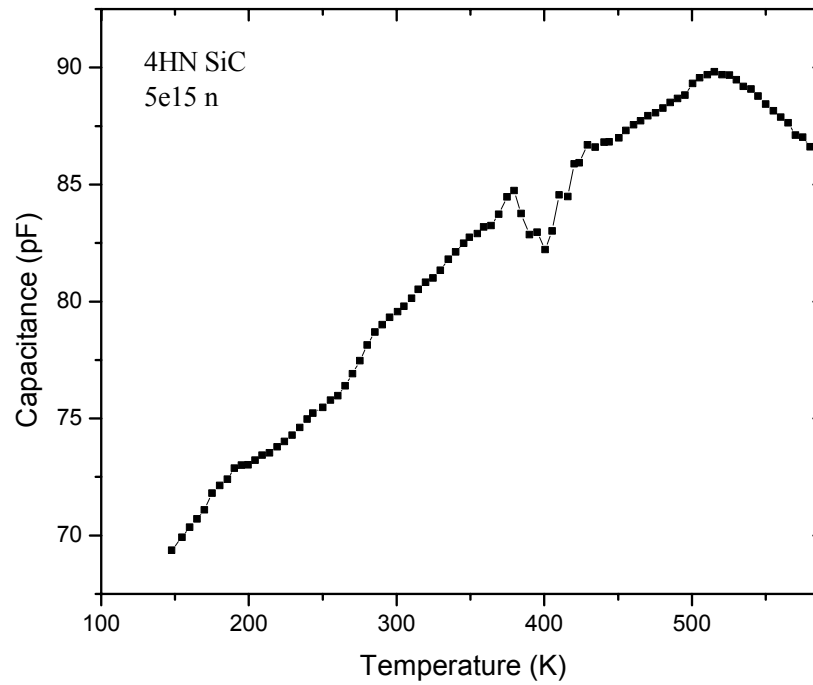


Figure 22: Observed Capacitance Roll-Over in Irradiated 4H-SiC

Another observation is the apparent capacitance rollover shown in Figure 22. This was not observed in slightly irradiated or as-grown samples. Theory suggests that capacitance should continue to increase as a function of temperature due to an increase in free thermal charges. The existence of the capacitance rollover may be explained by three different processes; an overall degradation in performance due to the increased number of Frenkel defects and vacancy-interstitial pairs, the dislocation sites may assist in a form of charge tunneling across the capacitor at higher temperatures, and compensation may be occurring as deeper acceptor levels begin to be ionized. This rollover may also contribute to an operational temperature limit on a device.

Early in the experiment, all samples were analyzed using a temperature range of 100 to 700 K. It was noticed, after the need to rerun one sample that the sample previously heated to 700 K had a much greater leakage current, to the point that some samples became too leaky for a second run. It is apparent that the thermal heating (annealing) of these samples to 700K for the time needed to complete the experiment permanently damaged not just a single contact but the entire sample. Since no appreciable defect site was detected above 600 K, all of the following samples were analyzed between 100 and 600 K and no further device damage was noted. Therefore, the expected activation temperature for a neutron-irradiated generation-recombination (G-R) center is between 600-700 K.

Many authors have also noted the strong impact of neutron bombardment on the dopant level, as it has been used as an n-type dopant technique (McLean, 1994). Table 6 is a listing of measured dopant levels as a function of 1 MeV neutron fluence as measured by C-V profiling.

Table 6: Dopant Level vs. Neutron Fluence in n-type SiC at Room Temp

1 MeV Neutron Fluence (n/cm²)	Dopant Level (N_D-N_A)
0	1.6E17
1E13	1.5E17
1E14	1.5E17
1E15	1.8E17
5E15	1.5E17
1E16	9E16

No clear trend in the change of dopant level was shown in the n-type material. This may be a result of the sensitivity of the measurements, but is most likely a result of saturation of free carriers already present in the highly nitrogen doped material.

n-type Hall Results

All the Hall effect data collected for this experiment was obtained at 300 K. No temperature dependent Hall information was collected due to unavailability of equipment. As a result, the information collected was at the same temperature as a major deep level trap site located in the DLTS phase of the experiment. Thus this major trap site may influence base line data. The location of this trap (305 K), most certainly could impact the value obtained during the Hall effect measurements. Thus general statements will be made about the data collected, but the data cannot be used to make quantified statements.

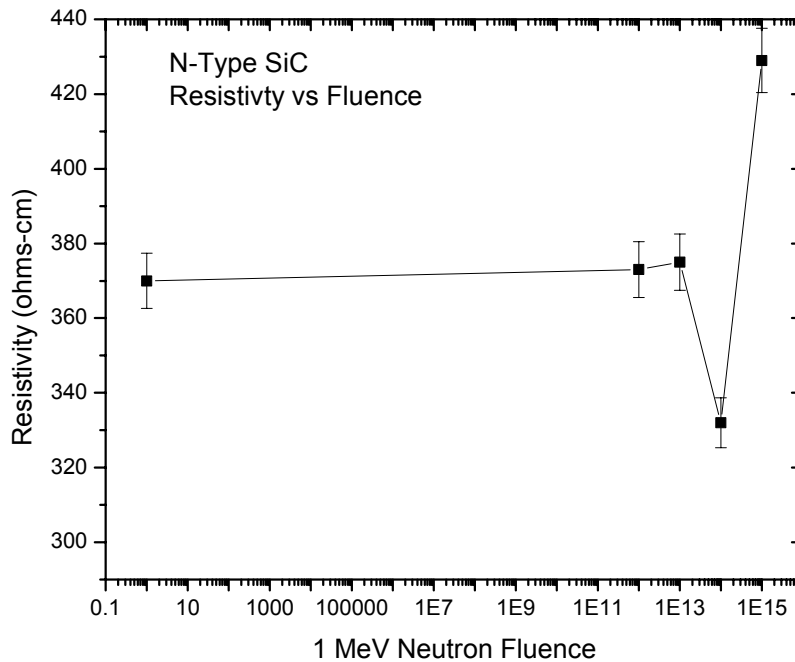


Figure 23: Resistivity vs. Fluence in n-type SiC

Figure 23 is a plot of the measured hall resistivity vs. fluence for n-type 4H SiC. Theory suggests that as the number of defect sites is increased, resistivity should increase accordingly. The data shows this to be the case but only in highly irradiated samples.

Figure 24 is a plot of the measured sheet carrier concentration vs. fluence for n-type 4H SiC. The measured values tend to agree with the carrier dopant levels reported earlier. It appears that as the fluence increases, the sheet carrier concentration also increases, until some other process begins to dominate such as; 1) carrier saturation (which limits the number of carriers), 2) increased number of dislocation sites (which may limit the number of free carriers), or 3) neutron annealing (Harris, 35). Then the total number of carriers begins to decrease.

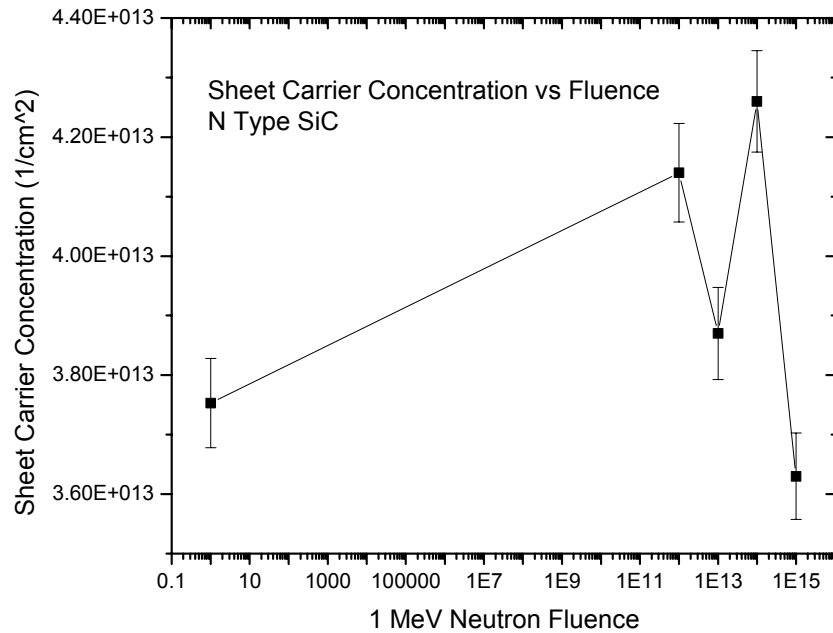


Figure 24: Sheet Carrier Concentration vs. Fluence for n-type SiC

Figure 25 depicts the measured Hall mobility as a function of fluence for n-type 4H SiC. Our expectation is that carrier mobility will decrease as a function of irradiation, as will carrier lifetime. The data collected does not clearly show this to be the case. In fact, it may show an increase in mobility due to tunneling taking place in the 305 K defect cluster, which could effectively lower the trap energy allowing the freer flow of charge.

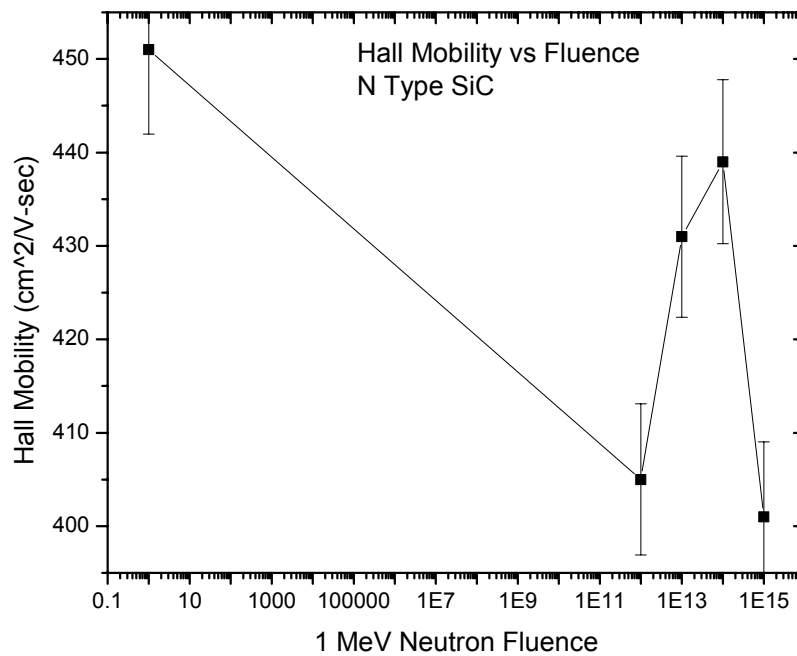


Figure 25: Hall Mobility vs. Fluence for n-type SiC

Figure 26 depicts the measured Hall coefficients for the n-type sample set. These values are presented only for comparison and may vary widely based upon temperature, as these measurements were made at the activation temperature for a major trap site.

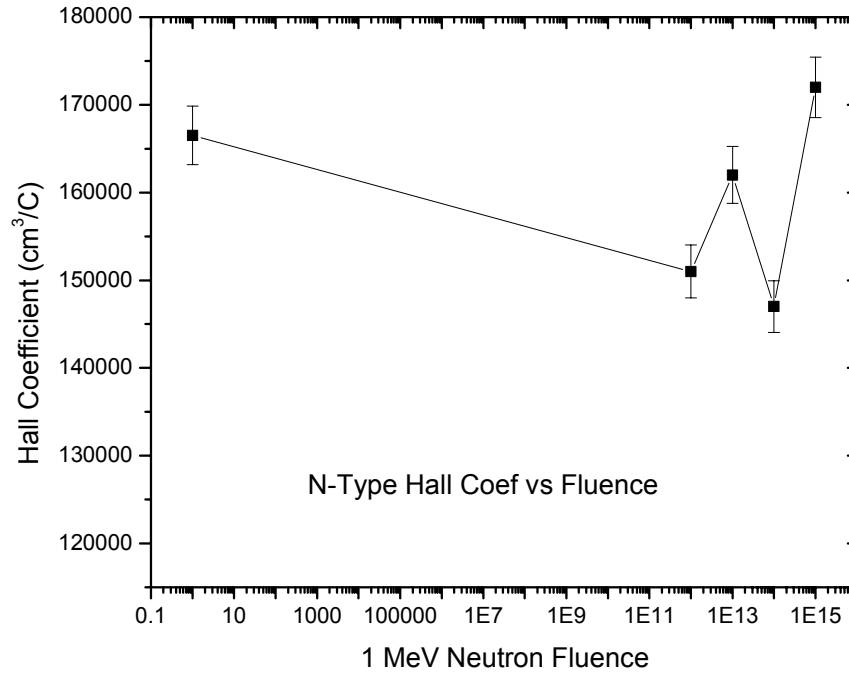


Figure 26: Hall Coefficient vs. Fluence for n-type SiC

P-Type Silicon Carbide

Observations of p-type SiC were made from test devices fabricated from two wafers of aluminum doped silicon carbide. The first wafer has a doping of $N_A - N_D = 1.5E18 \text{ cm}^{-3}$ and provides samples for both PL and DLTS analysis. The second wafer has a 5 μm Al doped epilayer of $N_A - N_D = 1.3E18 \text{ cm}^{-3}$ grown on an n-type SiC substrate. This configuration creates a narrow electrically isolated conductive channel required for quality Hall effect measurements.

p-type Photoluminescence Results

P-type SiC proved to be much more difficult than n-type to analyze using the PL technique due to the strong and broad luminescent peak centered at 2.9 eV that forms in

the middle of the region of interest. Figure 27 is the spectral response of an un-irradiated p-type 4H SiC control sample.

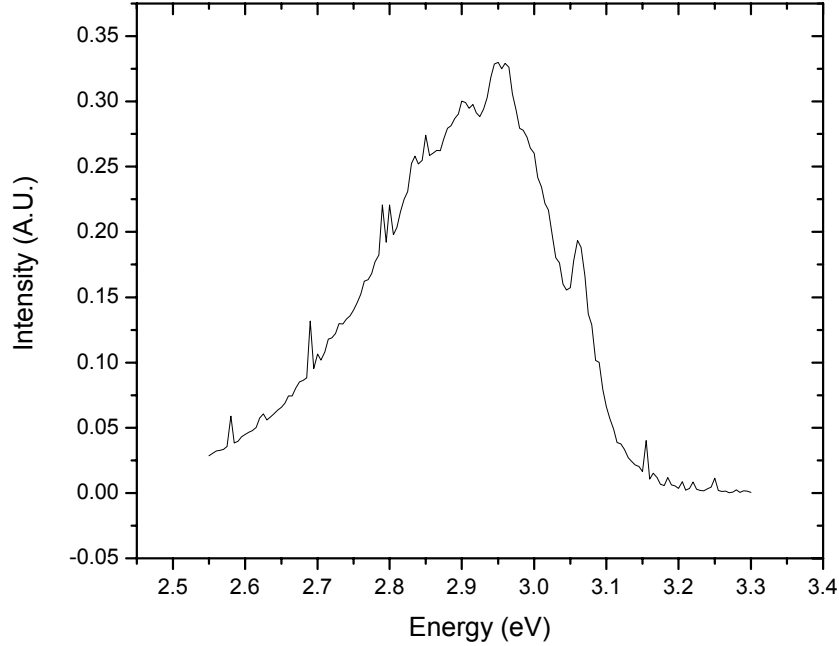


Figure 27: Un-irradiated PL Spectrum of p-type 4H Silicon Carbide

Previous studies found that two defect clusters commonly referred to as D_1 and D_2 may be attributed to excess carbon vacancies, dominate the spectral response, and limit the clear attribution of any particular feature (Harris, 35). These sites apparently remain stable even at high anneal temperatures, however, neutron irradiation appeared to impact the spectral appearance of this site. Figure 28 illustrates how the luminescent intensity of this peak decreases as a function of increasing 1 MeV neutron fluence.

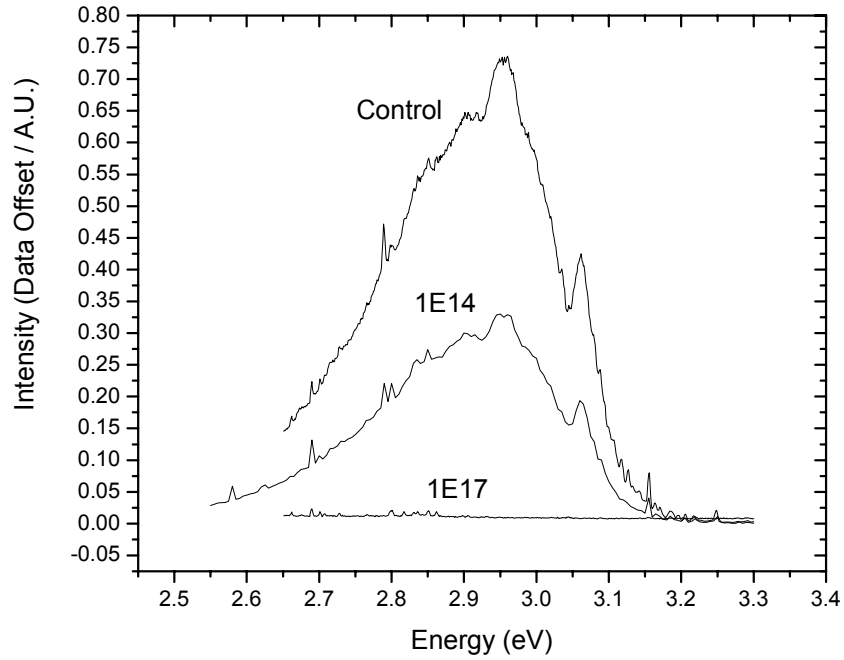


Figure 28: PL Response of p-type SiC to Various Irradiation Levels

As with n-type material, this may suggest that displacement damage within the crystal dominates the effects of this defect cluster and causes an excess of non-radiative free atoms that have no apparent luminescent properties. It has been suggested that anti-site defects may be the most common in as-grown material. However theory suggests these sites will be electrically inactive (Harris, 36).

p-type DLTS Results

DLTS observations on p-type 4H SiC were obtained using a wafer with an epi-layer of aluminum doping of $N_A - N_D = 1.5E18 \text{ cm}^{-3}$. As with n-type samples, measurements were conducted from 100 to 600 K using a computer controlled and triggered deep level transient spectrometer. Rate windows of similar magnitude were

also employed. Figure 29 shows the multiple rate window plot of a sample damaged with a 1 MeV neutron fluence of $1 \times 10^{15} \text{ n/cm}^2$.

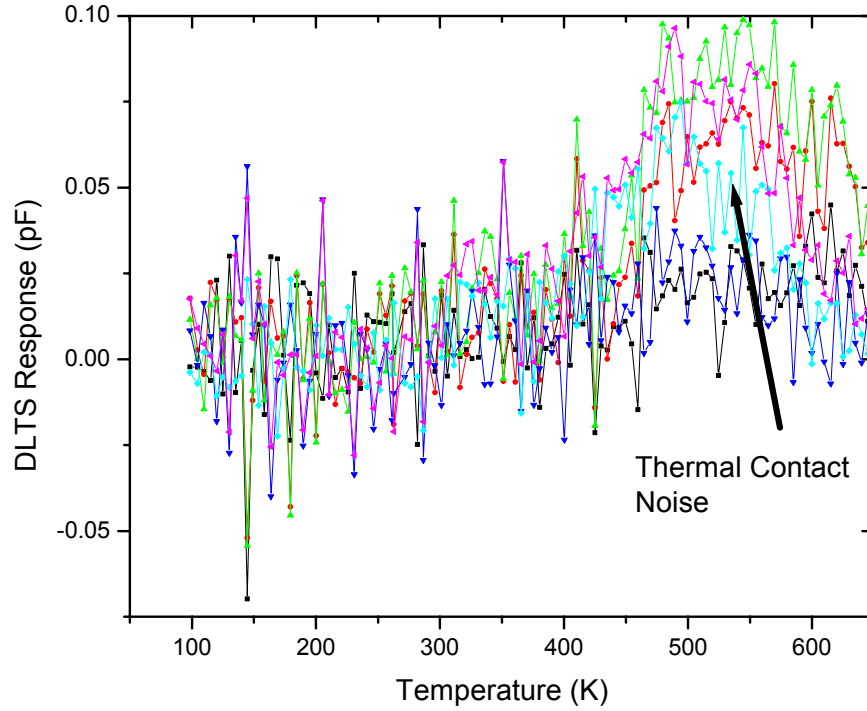


Figure 29: Measured DLTS Response of Irradiated p-type SiC

As shown the sample, in Figure 29 yielded no clear DLTS peaks. In fact no p-type sample yielded any discernable peak structure. The p-type sample produced fine devices with a turn on voltages of 0.7 volts and small $0.0015 \mu\text{A}$ leakage currents at $V_r = -6$ volts, but no defect structure was detected with this laboratory technique, as shown in Figure 30.

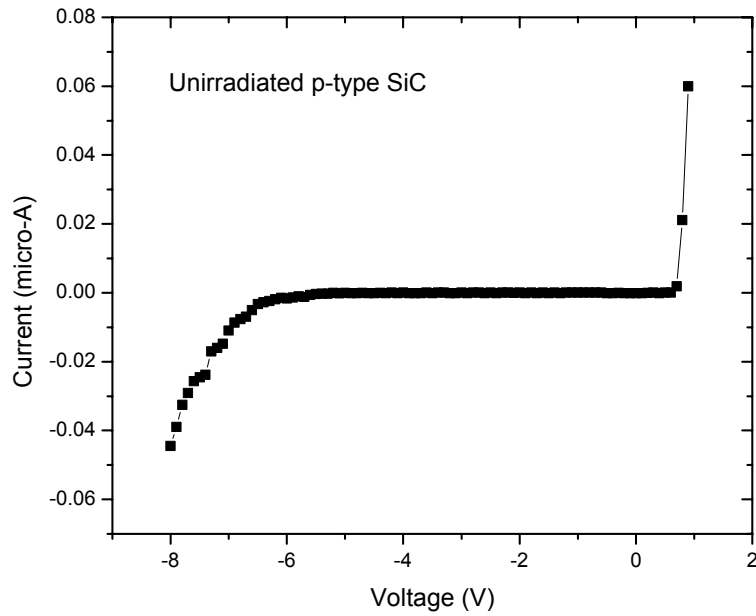


Figure 30: Measured I-V Curve of Un-irradiated p-type 4H SiC Schottky Diode

We attribute this to two possibilities. First, the p-type aluminum-doped samples have an even higher dopant concentration than the n-type nitrogen-doped samples. This high dopant is most likely masking defect structure that would be apparent in lower doped samples. Second, the masking of defect structure may be exacerbated by the diffusion of additional aluminum atoms brought about by the Al-Ti ohmic anneal process. This anneal time was kept to a minimum time and temperature (2 minutes at 900 K), but physical inspection of the contacts revealed deep metal-SiC amalgamation. Figure 31 shows the test strip used on the backside ohmic contact of a p-type 4H SiC sample to test the quality of an ohmic contact.



Figure 31: Back-Side Ohmic Contact on p-type SiC

The capacitance vs. temperature plots of the p-type samples revealed two interesting features, carrier freeze-out and capacitance rollover. Figure 32 shows a p-type sample that has been irradiated with a 1 MeV neutron fluence of $1\text{E}16 \text{ n/cm}^2$.

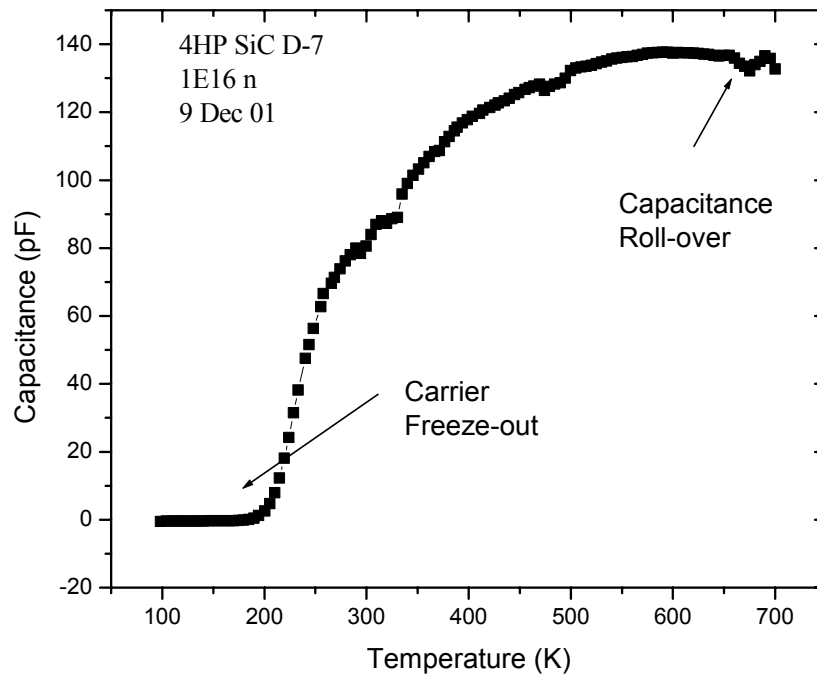


Figure 32: Measured Capacitance vs. Temperature Curve of p-type SiC

Firstly, freeze out of capacitance occurs just above 200 K. This effect was observed in all p-type samples. It appears that at low temperature the energy in the hole-rich material is low enough to effectively neutralize free carriers. This may indicate the existence of a large number of traps near the valence band of the material. Secondly, p-type samples showed a capacitance rollover in higher irradiated samples, although not as strong as in the n-type samples. This too may indicate the existence of Poole-Frenkel or other induced tunneling effects, assisting the detrapping of previously bound electrons (Blood *et al.*, 436).

As with n-type material, many authors have also noted the strong impact of neutron bombardment on the dopant level, as it has been used as an n-type dopant

technique (McLean, 1994). Table 7 is a listing of measured dopant levels as a function of 1 MeV neutron fluences in p-type 4H SiC, obtained through C-V measurements.

Table 7: Measured Dopant Level vs. Neutron Fluence in p-type SiC

1 MeV Neutron Fluence N/cm^2	Dopant Level ($N_A - N_D$)
0	2.0E18
1E13	2.0E18
1E14	1.9E18
1E15	1.8E18
1E16	3.5E17
1E17	1.0E13

Unlike the n-type material, the p-type material showed a much greater reaction to neutron bombardment. This can be attributed to the existence of electrons as a minority carrier, so electron saturation does not present the problem it does in the n-type material and more charge carriers are created.

p-type Hall Results

As with the n-type Hall data, all information was collected at 300 K. This may have tainted the quality of the data due to the possibility of the 305 K defect cluster that was very dominant in the n-type samples, and could have led to inconsistent room temperature base line data. The p-type material was much more resistive than the n-type SiC and its resistivity grew in response to greater neutron fluence, as was theoretically expected. This is shown in Figure 33, which depicts the measured resistivity vs. fluence for our p-type 4H SiC.

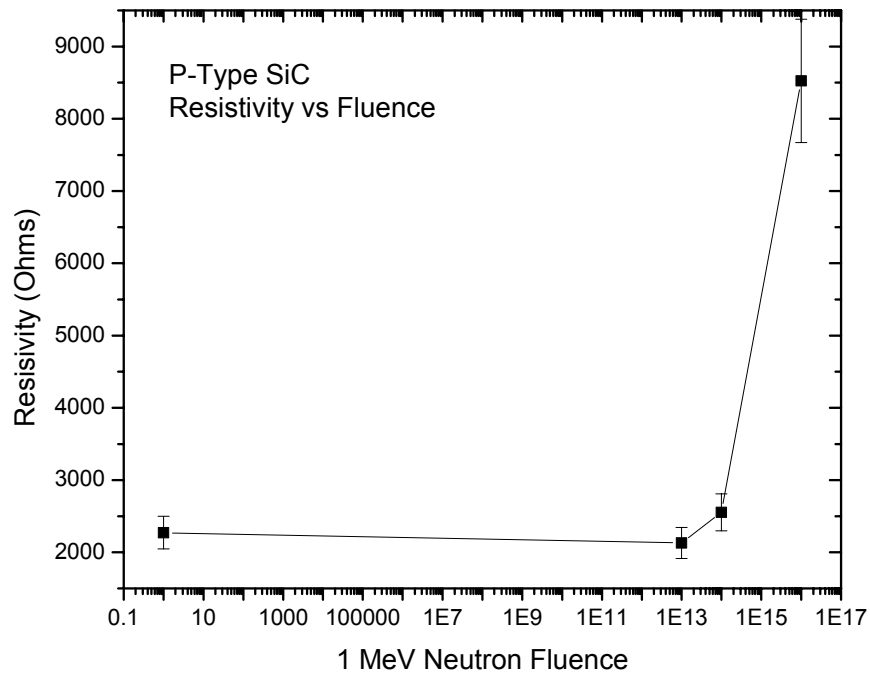


Figure 33: Measured Resistivity vs. Fluence for p-type SiC

As expected, it appears that the increase in dislocation defect sites made it more difficult for holes to travel through the material, causing an increase in resistivity. Figure 34 shows the measured value of sheet carrier concentration vs. fluence, which may show a decrease in free carriers as neutron fluence increases.

Figure 35 shows the measured Hall mobility as a function of exposed fluence, but no clear trends can be seen from this data.

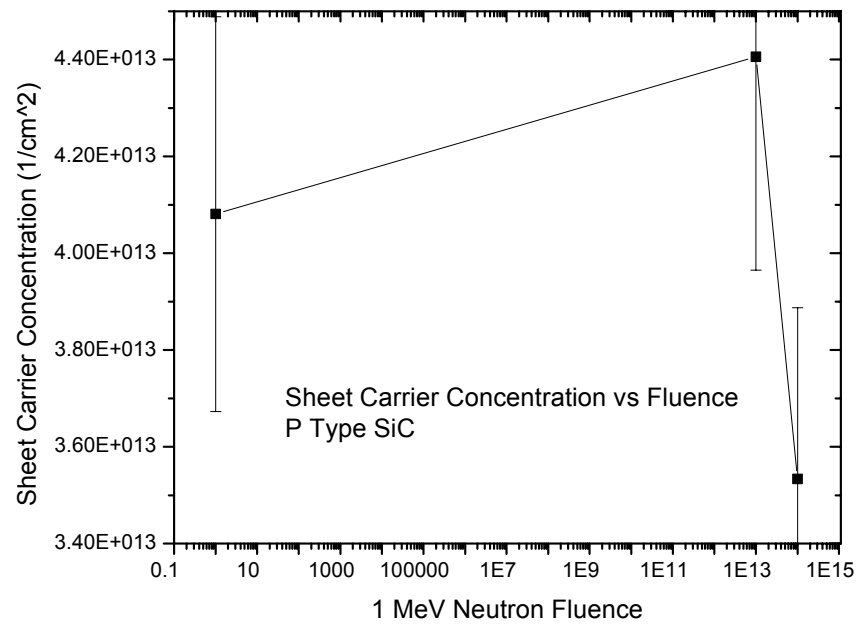


Figure 34: Measured Sheet Carrier vs. Fluence for p-type SiC

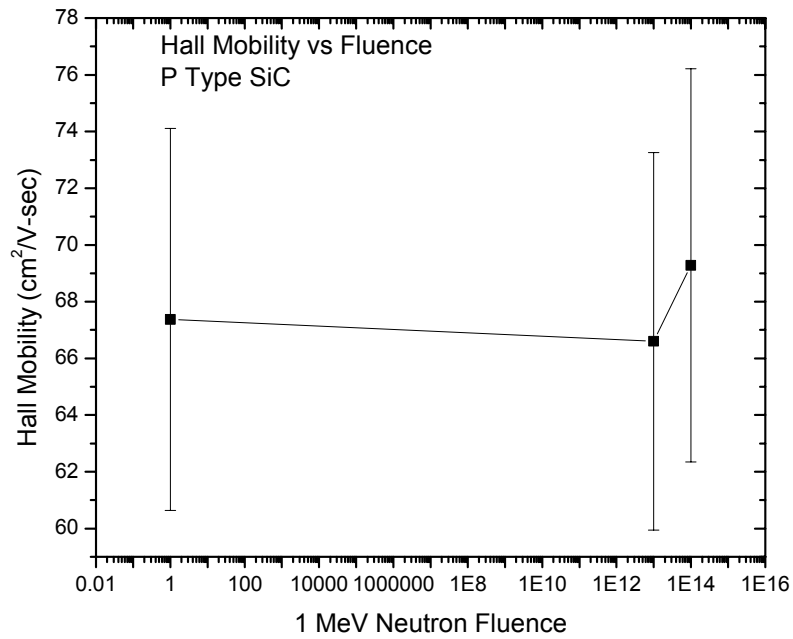


Figure 35: Measured Hall Mobility vs. Fluence for p-type SiC

Figure 36 depicts the measured Hall coefficient as a function of exposed fluence but as with Hall mobility lacks enough detail to promote any clear conclusions.

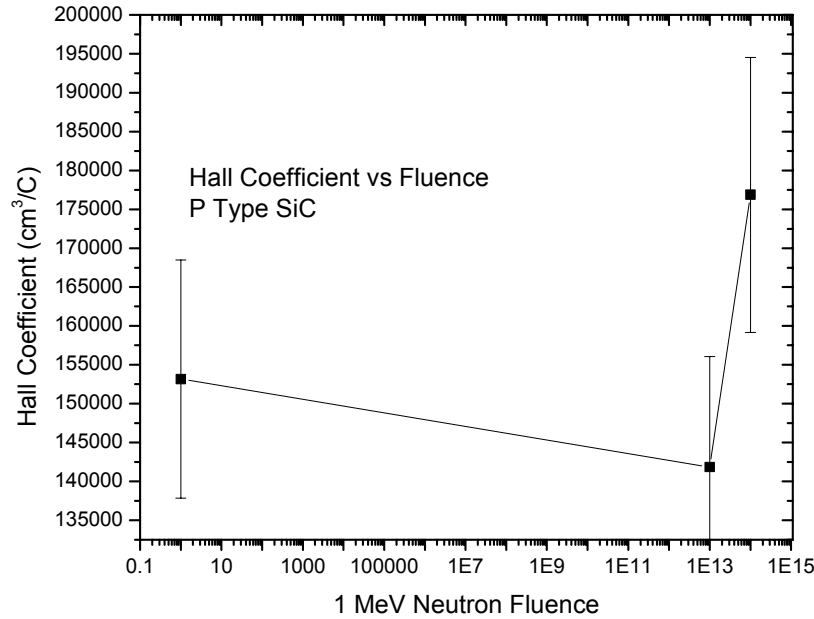


Figure 36: Measured Hall Coefficient vs. Fluence for p-type SiC

The absolute error for all p-type Hall measurements is 10%, while for n-type measurements it is 2%. The amount of error can be computed from the measured variance in Hall voltages. The variance is affected by the quality of the device contacts. Additionally, the input current was reduced from 1 mA to 1 μ A in order to make the measurements on the p-type material.

Other Observations

Silicon carbide in its as-grown state is a silvery semi-transparent material. Neutron bombardment causes it to become more cloudy in the same way as with neutron-irradiated glass. The n-type material, in particular, showed such a consistent clouding

that samples could be cataloged according to their exposed fluence based only on appearance.

Leakage current changes as a function of fluence were also observed. Leakage current is critical to good device performance. Table 8 lists the leakage current as a function of exposed fluence for the n-type 4H SiC Schottky diodes manufactured during this experiment.

Table 8: Measured Schottky Diode Leakage Current in n-type 4H SiC

Exposed Neutron Fluence (n/cm ²)	Negative 3 volt leakage current (μ A)
0	5
1E12	4
1E13	7
1E14	10
1E15	15
5E15	21
1E16	33
1E17	> 65

For this experiment, only diodes with leakage currents less the 50 μ A at -3 V could be used during DLTS measurements. P-type devices also showed superior performance as shown in Figure 37, which depicts a 4H p-type sample irradiated with $1\text{E}12$ n/cm². For this device, negative 3-volt leakage current is only 0.0036 μ A and a turn-on voltage of 0.3 volts.

Another useful measurement that was used to assist in determining an appropriate reverse bias voltage in DLTS is the carrier concentration vs. voltage graph as shown in Figure 38, which depicts the concentration for a 4H n-type sample irradiated to $1\text{E}14$ n/cm².

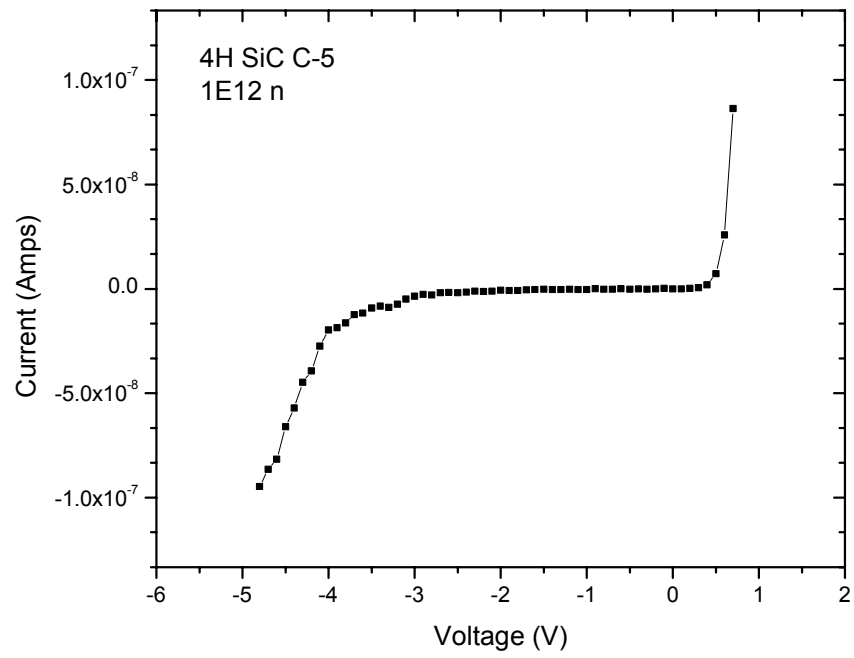


Figure 37: Measured I-V Curve for an Irradiated p-type Schottky Diode

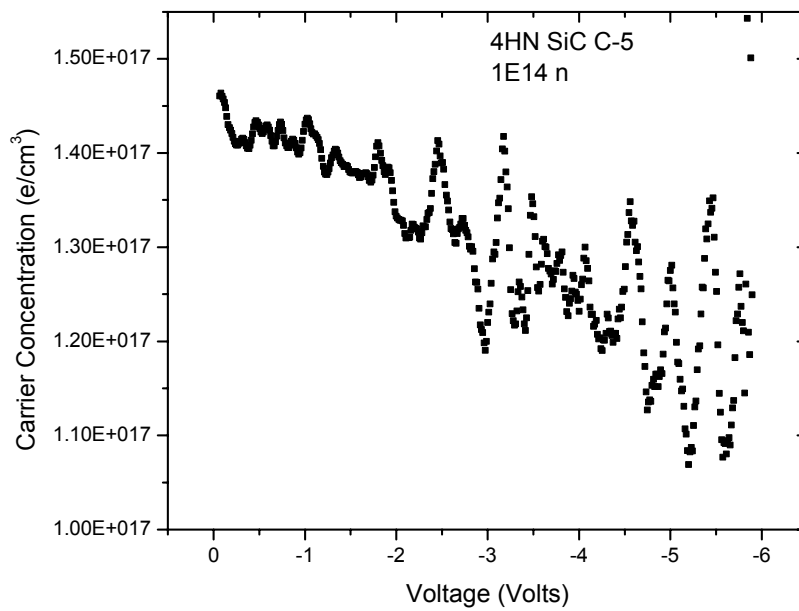


Figure 38: Measured Carrier Concentration Profile for a n-type Schottky Diode

V. Research Summary

In summary, this experiment consisted of three major parts. First a neutron bombardment phase was completed with the assistance of the Ohio State University research reactor staff. Secondly, a study was performed to determine the best method in which to fabricate the devices needed for analysis of the material. Lastly, photoluminescence (PL), deep level transient spectroscopy (DLTS), and Hall effect measurements were performed in order to determine material response to varying neutron fluences.

Of greatest importance is the demonstration that 4H silicon carbide was capable of forming good quality devices that demonstrated both a high tolerance to 1 MeV neutron fluences below $1\text{E}14\text{ n/cm}^2$, and did not exhibit a change in characteristics sufficient to breakdown until fluences greater than $1\text{E}16\text{ n/cm}^2$ were achieved. This suggests that quality devices can be formed with a neutron survivability of at least one order of magnitude greater than traditional silicon devices.

Conclusions

Photoluminescence

N-type PL experiments revealed the disappearance of the zero phonon lines (ZPLs) and their phonon replicas as a function of increased irradiation. This was attributed to the early dislocation of the bound neutral nitrogen donors within the crystal lattice due to the higher neutron cross section and the relatively weaker nitrogen bonds with the surrounding lattice structure.

P-type PL revealed the suppression of the broad dominant luminescent peak at 2.9 eV. This was attributed this to the increased number of vacancy-interstitial pairs and Frenkel defects affecting the dominance of the D1/D2 defect cluster and potentially the change in opacity causing the absorption of photon of these energies.

Deep Level Transient Spectroscopy

N-type DLTS revealed a number of deep level trap sites with the 305 K, 480 meV, 2×10^{16} site appearing most often across the varied neutron fluences.

Some trap sites may be masked by the relatively highly doped samples given the detection threshold of the deep level spectrometer.

Capacitance in highly irradiated n-type samples was observed to rollover around 510 K, could have resulted due to a variety of induced material changes, such and the possibility of charge tunneling at the Frenkel defect locations.

Test devices began to fail after prolonged exposure to a 700 K temperature environment (used in the original experimental procedures). This failure mode, along with the capacitance rollover, and higher initial leakage currents suggest potential sources of failure for irradiated 4H-SiC.

Hall effect

The interpretation of the Hall effect measurements was limited due to the lack of temperature dependant data, and only a few samples where examined. In general, measured Hall effect parameters suggest a general agreement with expected results.

Applications

The silicon carbide used for this study produced quality devices with neutron survivability of at least one order of magnitude greater then traditional silicon devices

(Northrop, 693). This observation implies that high quality devices can be manufactured that will be less vulnerable to changes, produced by neutron radiation and longer useful lifetime than is possible using traditional materials. This research also provides a platform for more advanced studies of the electrical properties of SiC, such as majority and minority carrier lifetimes needed to directly assist production and development efforts for both military and civilian applications.

Recommendations for Future Research

During the course of this experiment several interesting topics arose that lend themselves to additional research in this area.

A comprehensive temperature dependant Hall effect study should be performed in order to link observed PL and DLTS results and to reinforce and confirm conclusions drawn from this research.

A study that focuses on a tighter range of irradiated values would be beneficial in order to add statistical relevance to stated observations and assist in drawing conclusions on the more subtle effects of neutron fluence on device performance.

Many devices are dominated not by the majority carrier effects measured in this experiment but on the minority carrier effects. Therefore determination of the neutron minority and majority carrier constant for 4H-SiC would serve as an important modeling parameter needed in device design.

Since many of the conclusions of this study rely on the assumption that neutrons cause vacancy-interstitial pairs and Frenkel defects, a study that utilizes lab techniques capable of examining the post-irradiated lattice structure would be critical in determining if this is true and the rate at which they are created.

Lastly, this research showed that charge tunneling by several different mechanisms, such as the Poole-Frenkel effect, might exist in irradiated SiC. If sensitive measurements are taken using a finer range of neutron fluences, it may be possible to measure the reduction of trap energy as a function of increased fluence caused by these tunneling effects. Such a measurement would add greater our understanding of this phenomena.

Appendix A: Irradiation Test Plan

The Irradiation Test Plan is a separate document written to ensure the safety and viability of the neutron irradiation portion of the experiment, as such it is provided here as a reference largely in original form. Also note that during the study, devices fabricated from the sixth irradiation target group, 1×10^{17} n/cm² 1 MeV neutrons, proved to leaky for analysis so the seventh irradiation target group was changed from 1×10^{18} to a 5×10^{15} n/cm² 1 MeV neutron exposure.

Introduction

This document provides guidance for the irradiation experiment portion of the AFIT thesis ‘Determination of the Neutron Damage Constant for 4-H Silicon Carbide’. All aspects of planning, execution, radiation safety, and analysis have been included. This document is meant to outline everything that will need to happen in order to execute this phase of the research project.

This document begins with some background information about the materials to be tested, and some details about the irradiation facility. Next, the objectives, description, and priorities of this phase of testing are described in some detail. And last all details of planning for this phase of testing are spelled out in detail.

Background

Bulk 4H Silicon Carbide

In recent years, the activity in silicon carbide (SiC) has considerably increased due to the need for electronic devices capable of operation at high power levels and high temperatures. With its very high thermal conductivity (~ 5.0 W/cm), high-saturated

electron drift velocity ($\sim 2.7 \times 10^7$ cm/s) and high breakdown electric field strength (~ 3 MV/cm), SiC is a material of choice for high temperature, high voltage, high frequency and high power applications. The large Si-C bonding energy makes SiC resistant to chemical attack and radiation. SiC is needed to replace the existing semiconductor technologies of Si and GaAs, which cannot tolerate high temperatures and chemically hostile environments. With the possibility of working at high temperatures, high frequencies, and high voltages, SiC electronics opens a new generation of electronic equipment without cooling and transformers, offering a more effective and cheaper solution (LUS, 2001).

4-H growth SiC is a somewhat newer and as yet not fully characterized choice for potential device design, as such this will be the material tested. The wafers to be tested come from Cree, Inc. They are 4H-SiC, p ($0.5-1.5 \times 10^{18}$) and n ($.5-1.5 \times 10^{17}$)-type, research grade, 2" diameter wafers. From these wafers I will cut the wafer into 32 - .5 by .5 cm samples. From these a control group of 7 will be selected, which will not be irradiated. And a group of 25 will under go irradiation. In order to ensure completeness of data the irradiated group will be further divided into 7 groups, with each group having a different total dose requirement (see Irradiation Calculations). Table 9 is a list of sample requirements. Table 10 is a list of the seven-irradiation target groups:

Table 9: Bulk Sample Study

Target Dose	Sample Type	Hall	DLTS/CV	PL	Spare	Total
Control	n-Type SiC	0	3	3		6
	p-Type SiC	0	3	3		6
	n on p SiC	3	0	0		3
	p on n SiC	3	0	0		3
1	n-Type SiC	0	2	1		3
	p-Type SiC	0	2	1		3
	n on p SiC	2	0	0		2
	p on n SiC	2	0	0		2
2	n-Type SiC	0	2	1		3
	p-Type SiC	0	2	1		3
	n on p SiC	2	0	0		2
	p on n SiC	2	0	0		2
3	n-Type SiC	0	2	1		3
	p-Type SiC	0	2	1		3
	n on p SiC	2	0	0		2
	p on n SiC	2	0	0		2
4	n-Type SiC	0	2	1		3
	p-Type SiC	0	2	1		3
	n on p SiC	2	0	0		2
	p on n SiC	2	0	0		2
5	n-Type SiC	0	2	1		3
	p-Type SiC	0	2	1		3
	n on p SiC	2	0	0		2
	p on n SiC	2	0	0		2
6	n-Type SiC	0	2	1		3
	p-Type SiC	0	2	1		3
	n on p SiC	2	0	0		2
	p on n SiC	2	0	0		2
7	n-Type SiC	0	2	1		3
	p-Type SiC	0	2	1		3
	n on p SiC	2	0	0		2
	p on n SiC	2	0	0		2
Total		34	34	20		88

Table 10: Irradiation Targets

Target Number	Irradiation Fluence Goal
# 1	1E12
# 2	1E13
# 3	1E14
# 4	1E15
# 5	1E16
# 6	1E17
# 7	1E18

Radiation Source

The facility being used for this test is The Ohio State University Research Reactor (OSURR) in Columbus, Ohio (Ohio State, 2001). The reactor specifications are as follows:

Reactor Type	Open Pool
Thermal Power	500kW
Initial Criticality	March, 1961
Fuel	19.5% Enriched U_3Si_2
Cladding	Aluminum
Total ^{235}U Loading	~ 3.9kg
Moderator	Light Water
Primary Coolant	Light Water
Secondary Coolant	Ethylene Glycol
Experimental Facilities	- 1.3" Central Irradiation Facility (CIF) - Two 6" beam ports - 2" rabbit tube - 2.5" Auxiliary Irradiation Facility (AIF) - Graphite Thermal Column
Reactor Pool	- Depth: 20' - Length: 10' 7" - Width: 3' 8.5" - Volume: 5700 gallons - Liner: Epoxy-based paint

Due to the high flux requirements of the test the CIF will be the primary experimental port. The neutron spectrum for this port is included in Irradiation Calculations section.

Test Objectives

The objectives of this phase of the experiment are to safely and uniformly irradiate the SiC samples to the set total dose requirements. This will be accomplished using The Ohio State research reactor based upon the calculations contained in the Irradiation Calculations section. To be a success the resulting irradiated samples must:

- 1) Show minority carrier lifetime changes as compared to the control group.
- 2) Select enough groups to allow for comparison differences in lifetime values.

Test Description

Sample Preparation

The SiC wafers will be pre-characterized visually, optically (with a cross polarizer), and using a resistivity probe. The wafers will be cleaned and a photo resist will be applied to reduce surface contamination. The wafer will then be cut into the appropriate sized samples and then cleaned and labeled (see Experimental Equipment). Before being separated in irradiation bunches for transport each sample will be measured and weighed. The correct groups will be transported to The Ohio State University research reactor by POV.

Actions at Reactor Site

The samples will next be grouped (p and n type) together according to total dose goal. Each group will then be clad in a 4mm cadmium casing for thermal neutron absorption (bundle). Each bundle will be placed in the reactor CIF port for the required

time period ensuring the total dose goal has been met. Each bundle will be allowed to thermally cool and will then be checked for activation. Once it is determined that the samples are safe for release, the appropriate paperwork will be completed and the samples will be available for transport to the AFIT campus via military vehicle.

Post Irradiation Handling

The samples will be stored in building 470 if activated and in room 128A of building 644 if not activated. The samples will be used for Photoluminescence (PL), Deep Level Transient Spectroscopy (DLTS), Hall Effect (Hall), and Current-Voltage (CV) measurements needed to determine the changes in minority carrier lifetime and defect natures.

Samples designated for DLTS/CV measurements will be further processed by the application of Schottky contacts. Samples designated for Hall analysis will be further processed by the application of Ohmic van der Pauw contacts. Samples designated for PL analysis will undergo an additional cleaning process.

Test Priorities

The priorities of this phase of the experiment are as follows:

1. Achieve accurate irradiation levels among all samples.
2. Have enough target levels to have statistically sound results.
3. Ensure uniform irradiation of samples within a group.
4. Maintain cleanliness of samples in order to minimize activation and maximum suitability for analysis.

Radiation and Safety and Activation

Safety Plan

General Safety Requirements:

1. Do not eat, drink, smoke, or apply cosmetics in areas where unsealed radioactive materials are used.
2. Do not pipette solutions containing radioactive material by mouth.
3. Use disposable gloves while handling uncontained radioactive material.
4. Wash hands after working around uncontained radioactive material.
5. Wear lab coats or other protective clothing in case of a spill.
6. Be familiar with ALL operating procedures developed for use of radioactive material.
7. Use serviceable radiac equipment whenever appropriate.

AFIT Site:

1. As Low As Reasonably Allowable (ALARA), philosophy will be in affect at all times.
2. All required safety training/requirements will be complete prior to operation of any test equipment for characterization and/or data measurement. Training includes radiation, laser, clean room safety briefs and laser eye examination.
3. TLD radiation measurement devices will be worn by all personnel during set-up and measurement procedures. Portable radiation detectors will be used in the vicinity of all radioactive sources.
4. Rehearsal of measurement techniques may be necessary to ensure minimum exposure time. The use of radioactive markers will be used as needed.

Transportation:

1. TLD radiation measurement devices will be worn by all personnel when in the presence of potentially radioactive/activated material.
2. Portable pigs will be employed as shielding during transportation.

OSU Site:

1. As Low As Reasonably Allowable (ALARA) philosophy will be in affect at all times.
2. TLD radiation measurement devices will be worn by all personnel during set-up and measurement procedures. Portable radiation detectors will be used in the vicinity of all radioactive sources.
3. OSU Site specific restrictions will be followed at all times.

Travel Plan

In order to facilitate proper transportation of potentially radioactive materials between The Ohio State University Nuclear Reactor Facility in Columbus, Ohio and the AFIT campus, a GOV will be used to return all post-irradiated samples. This vehicle will be requested through the AFIT GOV coordinator prior to its use.

Post-Irradiation Analysis Plan

Following the irradiation of samples, samples will under go PL, DLTS/CV, and/or Hall analysis.

Points of Contact

The following are emergency POCs at WPAFB and within AFIT:

Participants: MAJ Kent Jones
Kent.Jones@afit.edu
255-3636 (4824)

Instructor: LTC James Petrosky
James.Petrosky@afit.edu
255-3636 (4600)

AFIT Radiation Safety Officer: MAJ Vincent Jodoin
Vincent.Jodoin@afit.edu
255-3636 (4506)

Base Radiation Safety Officer: Mr. Mark Mays
255-2010 (208)

OSU Contact: Mr. Joe Talnagi
Talnagi.1@osu.edu
(614) 688-8230

Irradiation Calculations

The following calculations were completed in MATHCAD and provided as follows:

Preliminary Dose Calculations: *As of: 20 September 2001*

Part I - Calculate the Dose Rate for un-shielded 4-H Silicon Carbide:

1) Fundamental constants used in SiC calculations:

$$\rho_{\text{SiC}} := 3.21 \cdot \frac{\text{gm}}{\text{cm}^3} \quad A W_{\text{SiC}} := \frac{28.0855 + 12.0107}{2} \cdot \frac{\text{gm}}{\text{mol}}$$

$$\begin{aligned} \text{barn} &\equiv 10^{-24} \cdot \text{cm}^2 \\ \text{eV} &\equiv 1.602 \cdot 10^{-19} \cdot \text{joule} \\ \text{rad} &\equiv 100 \cdot \frac{\text{erg}}{\text{gm}} \end{aligned}$$

$$\text{Mrad} \equiv 10^6 \cdot \text{rad}$$

$$N_A \equiv 6.022 \cdot 10^{23} \cdot \text{mol}^{-1}$$

2) Calculate atomic number density:

$$N_{\text{SiC}} := \frac{N_A \cdot \rho_{\text{SiC}}}{A W_{\text{SiC}}}$$

$$\text{Gy} \equiv 1 \cdot \frac{\text{joule}}{\text{kg}}$$

$$\text{rad} \equiv 0.01 \cdot \text{Gy}$$

$$N_{\text{SiC}} = 9.642 \times 10^{22} \text{ cm}^{-3}$$

$$\text{MeV} := 1 \cdot 10^6 \cdot \text{eV}$$

3) Load from file values for fluence, energy bin, and group average cross section:

Energy in eVs		Fluence at that energy		SiC Microscopic XS		Cd Microscopic XS	
Data ⁽⁰⁾ =	0	0	0	0	0	0	0
	0	1·10 ⁻⁴	0	0	33.16	0	4.597·10 ⁵
	1	1.05·10 ⁻⁴	1	0	24.975	1	2.374·10 ⁵
	2	1.1·10 ⁻⁴	2	0	17.988	2	2.322·10 ⁵
	3	1.15·10 ⁻⁴	3	0	16.219	3	2.27·10 ⁵
	4	1.2·10 ⁻⁴	4	0	15.811	4	2.224·10 ⁵
	5	1.27·10 ⁻⁴	5	0	15.606	5	2.178·10 ⁵
	6	1.35·10 ⁻⁴	6	0	15.402	6	2.084·10 ⁵
	7	1.42·10 ⁻⁴	7	0	14.779	7	2.039·10 ⁵
	8	1.5·10 ⁻⁴	8	0	14.468	8	1.995·10 ⁵
	9	1.6·10 ⁻⁴	9	0	14.156	9	1.916·10 ⁵
	10	1.7·10 ⁻⁴	10	0	13.672	10	1.873·10 ⁵
	11	1.8·10 ⁻⁴	11	0	13.43	11	1.83·10 ⁵
	12	1.9·10 ⁻⁴	12	0	13.187	12	1.792·10 ⁵
	13	2·10 ⁻⁴	13	0	12.797	13	1.754·10 ⁵
	14	2.1·10 ⁻⁴	14	0	12.465	14	1.681·10 ⁵
	15	2.2·10 ⁻⁴	15	0	11.983	15	1.644·10 ⁵

4) Compute the Macroscopic Cross Sections for Sic:

$$\mu_{SiC} := \text{Data}^{(2)} \cdot \text{barn} \cdot N_{SiC}$$

	0
0	3.197
1	2.408
2	1.734
3	1.564
4	1.524
5	1.505
6	1.485
7	1.425
8	1.395
9	1.365
10	1.318
11	1.295
12	1.272
13	1.234
14	1.202
15	1.155

$$\mu_{SiC} = \text{cm}^{-1}$$

5) Compute the Energy Fluence (Flux) for the Source:

$$\psi := \left(\left(\text{Data}^{(0)} \cdot \text{eV} \cdot \text{Data}^{(1)} \cdot \frac{1}{\text{cm}^2 \cdot \text{s}} \right) \right)$$

	0
0	0
1	0
2	0
3	0
4	0
5	0
6	0
7	0
8	0
9	0
10	0
11	0
12	0
13	0
14	0
15	0

$$\psi = \text{kg s}^{-3}$$

6) Compute the Mass Attenuation Coefficient for 4-H SiC:

$$\text{MAC} := \frac{\mu_{SiC}}{\rho_{SiC}}$$

	0
0	0.1
1	0.075
2	0.054
3	0.049
4	0.047
5	0.047
6	0.046
7	0.044
8	0.043
9	0.043
10	0.041
11	0.04
12	0.04
13	0.038
14	0.037
15	0.036

$$\text{MAC} = \text{m}^2 \text{kg}^{-1}$$

7) Calculate the Dose Rate for 4-H SiC:

$$\text{DoseRate}_{\text{SiC}} := \psi \cdot \text{MAC}$$

$$\text{DoseRate}_{\text{SiC}} = 153.53 \text{ kg}^{-1} \frac{\text{joule}}{\text{s}}$$

$$\text{DoseRate}_{\text{SiC}} = 1.535 \times 10^4 \frac{\text{rad}}{\text{s}}$$

$$\text{DoseRate}_{\text{SiC}} = 55.271 \frac{\text{Mrad}}{\text{hr}}$$

8) Find the average sample Mass:

$$\rho_{\text{SiC}} := 3.21 \cdot \frac{\text{gm}}{\text{cm}^3} \quad \text{SampleDimensions} := .5 \cdot \text{mm}^2 \cdot 470 \cdot 10^{-9} \cdot \text{m}$$

$$\text{SampleDimensions} = 2.35 \times 10^{-7} \text{ cm}^3$$

$$\text{Mass}_{\text{sample}} := \rho_{\text{SiC}} \cdot \text{SampleDimensions}$$

$$\text{Mass}_{\text{sample}} = 7.543 \times 10^{-7} \text{ gm}$$

Part II - Calculate the effect of Cadmium attenuation:

1) Fundamental constants used in Cd calculations:

$$\rho_{Cd} := 8650 \frac{\text{kg}}{\text{m}^3} \quad AW_{Cd} := 112.41 \frac{\text{gm}}{\text{mol}}$$

2) Calculate the atomic number density for Cd:

$$N_{Cd} := \frac{N_A \cdot \rho_{Cd}}{AW_{Cd}}$$

$$N_{Cd} = 4.634 \times 10^{22} \text{ cm}^{-3}$$

3) Calculate the Macroscopic cross section for Cd:

$$\mu_{Cd} := \text{Data}^{(3)} \cdot \text{barn} \cdot N_{Cd}$$

$$\mu_{Cd\text{Single}} := 144.84 \text{ barn} \cdot N_{Cd}$$

$$\mu_{Cd\text{Single}} = 671.182 \text{ m}^{-1}$$

4) Calculate the Mass Attenuation Coefficient for Cd:

$$MAC_{Cd} := \frac{\mu_{Cd}}{\rho_{Cd}}$$

$$MAC_{Cd\text{Single}} := \frac{\mu_{Cd\text{Single}}}{\rho_{Cd}}$$

$$MAC_{Cd\text{Single}} = 0.078 \text{ m}^2 \text{ kg}^{-1}$$

Not used in future calculations!!!

	0
0	2.13·10 ⁴
1	1.1·10 ⁴
2	1.076·10 ⁴
3	1.052·10 ⁴
4	1.031·10 ⁴
5	1.009·10 ⁴
6	9.656·10 ³
7	9.45·10 ³
8	9.243·10 ³
9	8.88·10 ³
10	8.679·10 ³
11	8.479·10 ³
12	8.303·10 ³
13	8.127·10 ³
14	7.791·10 ³
15	7.62·10 ³

$$\mu_{Cd} = \text{cm}^{-1}$$

	0
0	246.261
1	127.192
2	124.396
3	121.6
4	119.145
5	116.689
6	111.625
7	109.243
8	106.861
9	102.662
10	100.34
11	98.018
12	95.986
13	93.954
14	90.068
15	88.093

$$MAC_{Cd} = \text{m}^2 \text{ kg}^{-1}$$

5) Compute the thickness of Cd required to absorb all thermal flux:

$$\text{ActivityFinal} = \text{ActivityInitial} \cdot e^{-\mu_{Cd\text{Single}} \cdot \text{Thickness}} \quad \text{Page 185 eqn 8.43 Turner}$$

At the 1eV energy group assuming a 90% attenuation (which is much higher for lower energy groups)

$$X := .003432 \text{ m}$$

$$X = 3.432 \text{ mm}$$

Assume a 4 mil Cd Case

6) Compute the attenuated Neutron flux for a 4 mil Cd Case:

$$\psi_{Cd} := \overrightarrow{\left(\psi \cdot e^{-\mu_{Cd} \cdot 4 \cdot \text{mm}} \right)}$$

$\psi_{Cd} =$

	0
0	0
1	0
2	0
3	0
4	0
5	0
6	0
7	0
8	0
9	0
10	0
11	0
12	0
13	0
14	0
15	0

 kg s^{-3}

7) Calculate the dose rate for the cadmium shielded SiC:

$$\text{DoseRate}_{\text{SiCwithCd}} := \text{MAC} \cdot \psi_{Cd}$$

$$\text{DoseRate}_{\text{SiCwithCd}} = 50.356 \frac{\text{Mrad}}{\text{hr}}$$

Part III - Estimate the stopping distance for a 1 MeV Neutron in 4-H SiC:

1) Recall the fundamental constants for SiC from Part I:

$$\rho_{\text{SiC}} := 3.21 \cdot \frac{\text{gm}}{\text{cm}^3} \quad A_{\text{W}_{\text{SiC}}} := \frac{28.0855 + 12.0107}{2} \cdot \frac{\text{gm}}{\text{mol}}$$

2) Calculate atomic number density of SiC:

$$N_{\text{SiC}} := \frac{N_A \cdot \rho_{\text{SiC}}}{A_{\text{W}_{\text{SiC}}}}$$

$$N_{\text{SiC}} = 9.642 \times 10^{22} \text{ cm}^{-3}$$

3) Calculate the Macroscopic cross section for a 1 MeV Neutron in SiC:

$$\mu_{1\text{MeVSiC}} := N_{\text{SiC}} \cdot 3.839825 \text{ barn}$$

$$\mu_{1\text{MeVSiC}} = 0.37 \text{ cm}^{-1}$$

4) Compute the thickness of SiC needed to stop 99% of 1 MeV Neutrons:

$$\text{ActivityFinal} = \text{ActivityInitial} \cdot e^{-\mu_{1\text{MeVSiC}} \cdot \text{Thickness}} \quad \text{Page 185 eqn 8.43 Turner}$$

At the 1MeV energy group assuming a 99% attenuation

$$X := 12.44 \text{ cm}$$

$$X = 124.4 \text{ mm}$$

For a 99.9% attenuation

$$X := 18.6696 \text{ cm}$$

And for a 99.999 % attenuation

$$X := 31.116 \text{ cm}$$

This result satisfies a question from the thesis committee and shows I can stack samples to some degree in my test apparatus.

Part IV - Neutron Spectrum Un-Folding:

To remain consistant with published works we need to express the neutron fluence in terms of a single energy group. Most often the spectrum is "normalized" to reflect the 1-MeV contribution, so that is what I will attempt to do.

1) Theory and general equations:

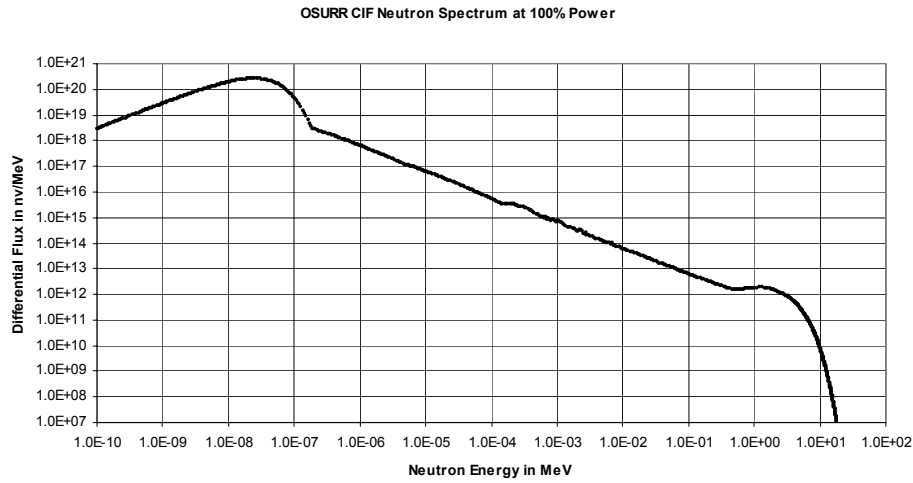
As shown previously

$$\text{DoseRate} = \psi(e) \cdot \left(\frac{\mu(e)}{\rho} \right)$$

To be exactly correct

$$\text{DoseRate} = \int_0^{E_{\max}} \psi(e) \cdot \left(\frac{\mu(e)}{\rho} \right) dE$$

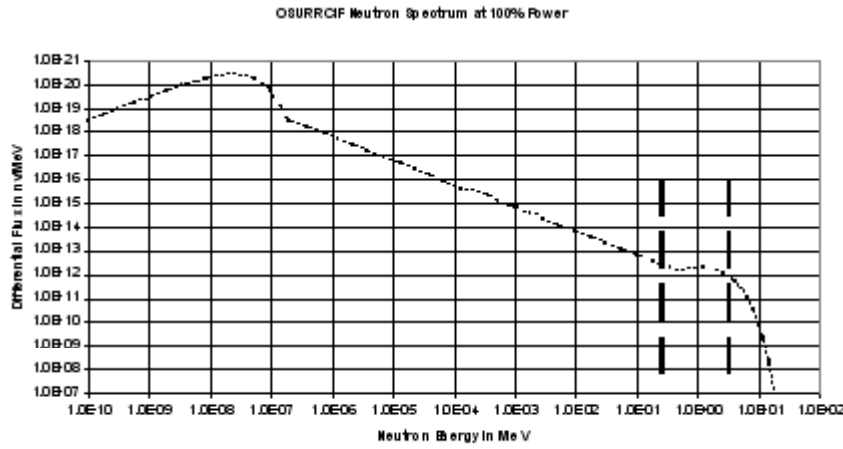
The spectrum of the source (Ψ) looks like this:



We then can discretize this in energy bins to become

$$\text{DoseRate} = \sum_{E=1}^{E_{\max}} \psi(e) \cdot \left(\frac{\mu(e)}{\rho} \right) \cdot E$$

But we want to express the Dose Rate as a function of only the 1MeV component of energy, which looks like:



And can be discretized to look like:

$$\text{DoseRate} = \psi(1\text{MeV}) \cdot \left(\frac{\mu(1\text{MeV})}{\rho} \right) \cdot (1\text{MeV})$$

Now we note that we can set the two discretized equations equal to each other and solve for the 1 MeV Energy Flux Density (Intensity) term which will allow further comparison to published work.

$$\psi(1\text{MeV}) = \frac{\sum_{E=1}^{E_{\text{max}}} \psi(e) \cdot \left(\frac{\mu(e)}{\rho} \right) \cdot E}{\left[\left(\frac{\mu(1\text{MeV})}{\rho} \right) \cdot (1\text{MeV}) \right]}$$

2) Calculate the 1 MeV Energy Flux Density (Intensity) w/o Cadmium:

$$\mu_{1\text{MeV}} := 3.8398254 N_{\text{SiC}} \cdot \text{barn}$$

$$\Psi_{1\text{MeV}} := \frac{\text{DoseRate}_{\text{SiC}}}{\frac{\mu_{1\text{MeV}}}{\rho_{\text{SiC}}} \cdot 1 \cdot \text{MeV}}$$

$$\Psi_{1\text{MeV}} = 8.309 \times 10^{16} \text{ m}^{-2} \text{ s}^{-1} \quad \text{mho}$$

3) Calculate the 1 MeV Energy Flux Density (Intensity) w/Cadmium:

$$\mu_{1\text{MeV}\text{Cd}} := 6.1 \cdot \text{barn} \cdot N_{\text{Cd}}$$

$$\Psi_{1\text{MeV}\text{withCd}} := \frac{\text{DoseRate}_{\text{SiCwithCd}}}{\left(\frac{\mu_{1\text{MeV}}}{\rho_{\text{SiC}}} \cdot 1 \cdot \text{MeV} \right)} \quad \text{Note lack of Cd attenuation in denominator}$$

$$\Psi_{1\text{MeV}\text{withCd}} = 7.57 \times 10^{16} \text{ m}^{-2} \text{ s}^{-1} \quad \text{Note this is incorrect due to lack of Cd term in denominator}$$

$$\Psi_{1\text{MeV}\text{withCd}} := \frac{\text{DoseRate}_{\text{SiCwithCd}}}{\left(\frac{\mu_{1\text{MeV}}}{\rho_{\text{SiC}}} \cdot 1 \cdot \text{MeV} \cdot e^{-\mu_{1\text{MeV}\text{Cd}} \cdot 4 \cdot \text{mm}} \right)}$$

$$\Psi_{1\text{MeV}\text{withCd}} = 8.476 \times 10^{16} \text{ m}^{-2} \text{ s}^{-1} \quad \text{Note the hardened intensity}$$

$$\Psi_{1\text{MeV}\text{withCd}} = 8.476 \times 10^{12} \text{ cm}^{-2} \cdot \text{s}^{-1} \quad \text{Which is in units appropriate for comparison}$$

4) Devise a test to check values:

If

$$\text{DoseRate}_{\text{SiCwithCd}} = 50.356 \frac{\text{Mrad}}{\text{hr}}$$

Then test must be equal:

$$\text{Test} := \frac{\mu_{1\text{MeV}}}{\rho_{\text{SiC}}} \cdot 1 \cdot \text{MeV} \cdot e^{-\mu_{1\text{MeV}} \text{Cd} \cdot 4 \cdot \text{mm}} \cdot \Psi_{1\text{MeVwithCd}}$$

$$\text{Test} = 50.356 \frac{\text{Mrad}}{\text{hr}}$$

Which it is so I have done step 3 correctly.

Part V - Calculate the Irradiation times required to meet targeted total fluence

$$\text{Target1} := 1 \cdot 10^{12} \cdot \frac{1}{\text{cm}^2} \quad \text{Target2} := 1 \cdot 10^{14} \cdot \frac{1}{\text{cm}^2} \quad \text{Target3} := 1 \cdot 10^{16} \cdot \frac{1}{\text{cm}^2} \quad \text{Target4} := 1 \cdot 10^{18} \cdot \frac{1}{\text{cm}^2}$$

$$\text{Time1} := \frac{\text{Target1}}{\Psi_{1\text{MeVwithCd}}} \quad \text{Time2} := \frac{\text{Target2}}{\Psi_{1\text{MeVwithCd}}} \quad \text{Time3} := \frac{\text{Target3}}{\Psi_{1\text{MeVwithCd}}} \quad \text{Time4} := \frac{\text{Target4}}{\Psi_{1\text{MeVwithCd}}}$$

$$\begin{aligned} \text{Time1} &= 0.118\text{s} & \text{Time2} &= 11.797\text{s} & \text{Time3} &= 1.18 \times 10^3 \text{s} & \text{Time4} &= 1.18 \times 10^5 \text{s} \\ & & & & \text{Time3} &= 19.662\text{min} & \text{Time4} &= 1.966 \times 10^3 \text{min} \\ & & & & & & \text{Time4} &= 32.771\text{hr} \end{aligned}$$

These are the values used in the test

Experimental Equipment

1. Research reactor



Figure 39: OSU Reactor Core

2. SiC Samples (marked and separated)

1 – 28 DLTS/CV

2 – 14 PL

3 – 28 Hall

3. Personnel TLD's

4. Irradiation Test Plan w/Supporting documents

5. Sample Handling Device

6. Lap Top Computer

7. Cadmium Casing (Provided by OSU)

8. POV for pre-irradiation trip

9. GOV for post-irradiation trip

Sample Preparation and Wafer Utilization

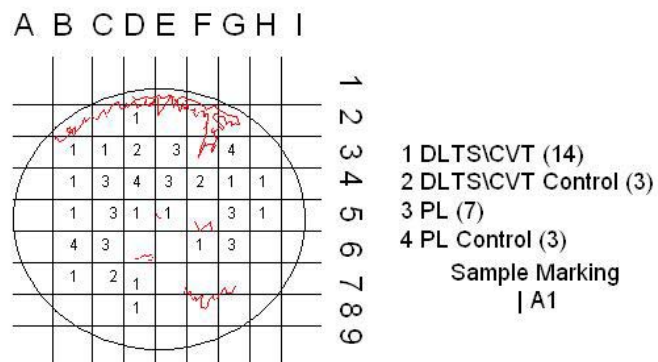
Sample Preparation List

1. Select/Sign for Wafers
2. Conduct visual and cross-polarizing inspection
3. Clean wafers
 - Place on spinner at 1000 RPM
 - Apply Trichloroethylene (TCE $\text{ClCH}_2\text{CCL}_2$) for 10 count
 - Apply ACETONE (CH_3COCH_3) for 10 count
 - Apply Methanol (CH_3OH) for 10 count
 - Dry with Nitrogen
4. Apply Photoresist
 - Apply a liberal amount of 1813 photoresist
 - Spin at 4000 rpm for 30 seconds
 - Place on drying plate at 100C for 4 min
5. Cut wafers
 - Mount wafers on cutting block with crystal bond
 - Mount cutting block on saw and cut into 5 mm square samples
6. Clean/mark samples
 - Repeat step 3 using pyrex dishes instead of spinner
 - Use diamond scribe to etch sample identification on back-side
 - Bag each sample with appropriate identification

Samples Required

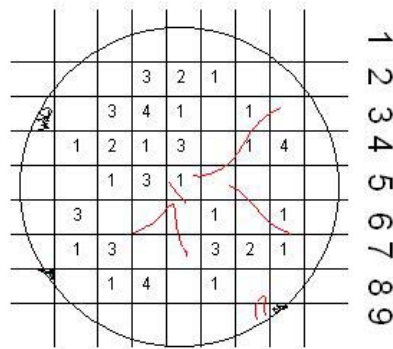
- From both n and p type wafers
 - 14 DLTS/CVT (irradiated)
 - 7 PL (irradiated)
 - 3 DLTS/CVT Control
 - 3 PL Control
 - **27 samples each**
- From both n/p and p/n wafers
 - 14 Hall
 - 3 Hall Control
 - **17 samples each**

Wafer # AQ0529-04 (4HP)



Wafer # AG0746-01 (4HN)

A B C D E F G H I

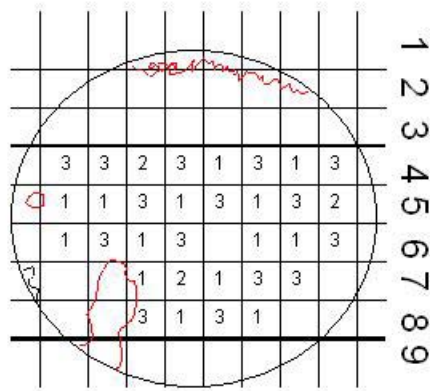


- 1 DLTS\CVT (14)
- 2 DLTS\CVT Control (3)
- 3 PL (7)
- 4 PL Control (3)

Sample Marking
A1 |

Wafer # AQ0523-09 (4HN/P)

A B C D E F G H I J

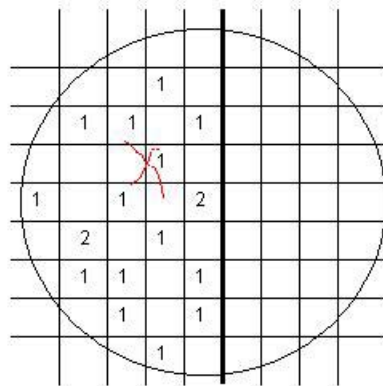


- 1 Hall (14)
- 2 Hall Control (3)
- 3 Other (15)

Sample Marking
A1

Wafer # XL0990-01 (4HP/N)

A B C D E F G H I



1
2
3
4
5
6
7
8
9

1 Hall (14)

2 Hall Control (2)

(one control yet selected)

2

Sample Marking

A1

Appendix B: Device Fabrication

The following are the “recipe cards” used in the preparation of samples during the experiment:

Sample Clean

1. Place on spinner at 1000 RPM
2. Apply Trichloroethylene (TCE $\text{ClCH}_2\text{CCl}_2$) for 10 count
3. Apply ACETONE (CH_3COCH_3) for 10 count
4. Apply Methanol (CH_3OH) for 10 count
5. Dry with Nitrogen (N_2)

Wafer Cut & Mark

1. Apply Photoresist
 - Apply a liberal amount of 1813 photoresist
 - Spin at 4000 rpm for 30 seconds
 - Place on drying plate at 100C for 4 min
2. Cut wafers
 - Mount wafers on cutting block with crystal bond
 - Mount cutting block on saw and cut into 5 mm square samples
3. Clean/mark samples
 - Repeat Sample Clean steps using pyrex dishes instead of spinner
 - Use diamond scribe to etch sample identification on back-side
4. Bag each sample with appropriate identification

Oxide Acid Etch

1. Complete Sample Clean steps
2. Using a beaker preheat a 3:1 aqua-regia ($\text{HCL}:\text{HNO}_3$) solution to 100°C on hot plate.
3. Add sample to be etched and swirl slightly until samples stop bubbling (approximately 5 min)
4. Remove samples from acid and rinse with at least 10 beakers of deionized water
5. Dry samples with N_2

Ohmic Backside Contacts

1. Complete Oxide Acid Etch
2. Mount with pressure contacts to evaporator mounting bracket
3. Apply uniform thickness of metal to entire backside of sample, 2000 Å Ni for N-type samples and 2000 Å Al/Ti (9:1, 200 Å Ti followed by 1800 Å Al) for P-type samples

Ohmic van der Pauw Contacts

1. Complete Oxide Acid Etch
2. Mount with pressure contacts to Hall evaporator mounting bracket
3. Apply uniform thickness of metal to entire front of sample, 2000 Å Ni for N-type samples and 2000 Å Al/Ti (9:1, 200 Å Ti followed by 1800 Å Al) for P-type samples
4. Place samples in petri dish with ACETONE
5. Place dish in ultrasonic bath until liftoff is complete

6. Clean with 10 count ACETONE, followed by 10 count Methanol, followed by N₂ dry

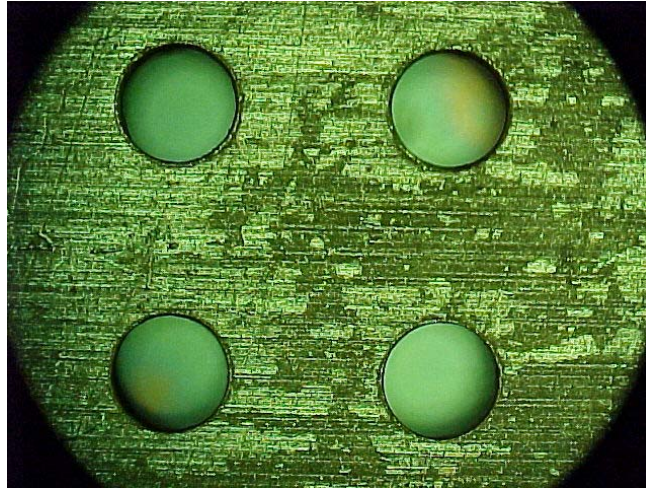


Figure 40: Ohmic van der Pauw Contacts (under mask)

Contact Anneal

1. Using tube furnace or RTA place sample in sample tray metal up
2. Anneal for 5 min at 1100°C for N-type and 2 min at 900°C for P-type

Rectifying Schottky Contacts

1. Complete Sample Clean (omitting TCE)
2. Place on spinner and apply liberal amounts of 1813 photo-resist
3. Spin at 7000 RPM for 30 sec
4. Bake on hot plate for 5 min at 100°C
5. Exposure sample using a DLTS mask in the mask aligner for 30 sec
6. Rinse at 1000 RPM with 351 developer solution (5:1, 5 parts deionized water and 1 part 351 developer) for 30 sec
7. Rinse with deionized water and dry with N₂
8. Bake on hot plate for 5 min at 100°C

9. Mount with pressure contacts to evaporator mounting bracket
10. Apply uniform thickness of metal to entire front of sample, 2000 Å Ti for both n- and p-type samples
11. Place samples in petri dish with ACETONE
12. Place dish in ultrasonic bath until liftoff is complete
13. Clean with 10 count ACETONE, followed by 10 count Methanol, followed by N₂ dry

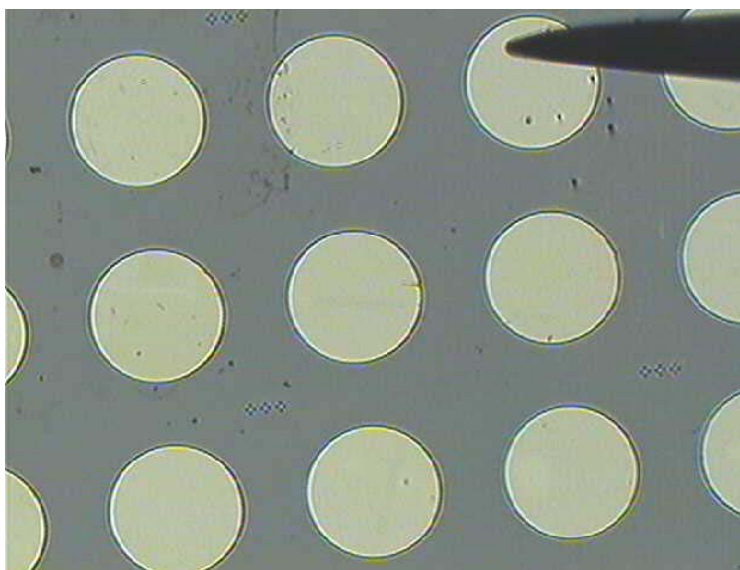


Figure 41: Rectifying Schottky Contacts

Bibliography

- Blood P. and Orton J.W. *The Electrical Characterization of Semiconductors: Majority Carriers and Electron States*. Academic Press Inc, Harcourt Brace Jovanovich, 1992.
- Borchi E., Bruzzi M., Dezillie B., Lazanu S., Li Z., and Pirollo S. "Hall Effect Analysis in Irradiated Silicon Samples with Different Resistivities," IEEE Transactions on Nuclear Science, Vol. 46 No. 4, August 1999.
- Braunig D., Fritsch D., and Lehmann B. "Radiation-Induced Displacement Damage in Silicon Carbide Blue Light-Emitting Diodes," IEEE Transactions on Nuclear Science Vol. 39, June 1992.
- Chapman, Stephen J. FORTRAN 90/95 for Scientists and Engineers. WCB/McGraw-Hill, 1998.
- Cree, Inc., "Offer and Agreement for Sale of Products," Technical information provided on bill of sale, 24 April 2001.
- Crockett, Heather C. "Analysis of Surface and Bulk Defects in 4H-Silicon Carbide Induce by Proton Irradiation," Masters Thesis, AFIT/GNE/ENP/02M-01, (Unpublished), 2002.
- Gfroerer, Timothy H. "Photoluminescence in Analysis of Surfaces and Interfaces," *Encyclopedia of Analytical Chemistry* Chichester: John Wiley & Sons Ltd, 9209-9231, 2000.
- Harris, Gary L. *Properties of Silicon Carbide*. The Institution of Electrical Engineers (INSPEC), 1995.
- Lebedev, A. A. "Deep Level Centers in Silicon Carbide: A Review," *American Institute of Physics*, Volume 33, Number 2, 1999.
- Linköping University of Sweden (LUS), "Silicon Carbide," Technical information provided on web page.
<http://www.ifm.liu.se/matephys/AAnew/research/sicpart/sicindex.html> 26 May 2001.
- Ma, T. P., Dressendorfer Paul V., and Kerns Sherra E. *Ionizing Radiation Effects in MOS Devices and Circuits*. John Wiley & Sons, New York, 1989.
- McLean F.B., McGarrity J.M., and Scozzie C.J., "Analysis of Neutron Damage in High-Temperature Silicon Carbide JFETs," IEEE Transactions on Nuclear Science, Vol. 41, No. 6, December 1994.

- Messenger, George C. and Ash, Milton S. *The Effects of Radiation on Electronic Systems* (2nd Edition). Van Nostrand Reinhold, New York, 1992.
- National Institute of Standards and Technology (NIST), Electronics and Electrical Engineering Laboratory, Semiconductor Electronics Division, Technical information provided on web page. <http://www.eeel.nist.gov/812/hall.html> 20 December 2001.
- Neudeck, Philip G. "SiC Technology," *NASA Lewis Research Center*, M.S. 77-1, Cleveland OH, 1998.
- Northrop, John *Handbook of Nuclear Weapon Effects*. Defense Special Weapons Agency, (Distribution Limited), 1996.
- Schroder, Dieter K. *Semiconductor Material and Device Characterization*. Jon Wiley & Sons, INC. 1998.
- Schueneman, Richard A. "Oxidation at Surfaces of Uranium Oxide Particles," Master Thesis, AFIT/GNE/ENP/01M-05, Air Force Institute of Technology, 2001.
- Scott, Michael B. *Electrical and Optical Characterization of Intrinsic and Ion-Implantation Induced Defects in 6H- and 4H-SiC* PhD Dissertation, AFIT/DS/ENP/99-04, Air Force Institute of Technology, 1999.
- Srour, J.R., Long, D.M., Millward D.G., Fitzwilson R.L., and Chadsey W.L. *Radiation Effects on and Dose Enhancement of Electronic Materials*. Noyes Publications, New Jersey 1984.
- Summers, Geoffrey P. "Displacement Damage: Mechanisms and Measurements," Naval Research Laboratory, NSREC Short Course Notes, 1992.
- Sze, S. M. *Semiconductor Devices Physics and Technology*. Bell Telephone Laboratories Inc., John Wiley & Sons, 1985.
- Technical University of Berlin (TUB), "Deep Level Transient Spectroscopy," Technical information provided on web page. http://sol.physik.tu-berlin.de/htm_reza/DLTS.HTM 28 February 2001.
- The Ohio State University, Technical information provided on web page. <http://www-nrl.eng.ohio-state.edu/facilities/reactor.html> 14 September 2001.
- Turner, James E. *Atoms, Radiation, and Radiation Protection*. Second Edition, New York: John Wiley & Sons Inc. 1995.
- University of Manchester (UM), "Laplace DLTS...An Overview," Technical information provided on web page. <http://www.mcc.ac.uk/cem/laplace/laplace.html> 4 March 2001.

Van Lint V. A., Gigas G., and Barengoltz, "Correlation of Displacement Effects
Produced by Electrons, Protons, and Neutrons in Silicon," IEEE Transactions on
Nuclear Science, Vol NS-22, No. 4, December 1975.

Vita

MAJ Kent T. Jones was born _____ in Madelia, Minnesota. In 1989, he was awarded a Bachelor of Science degree in Electrical Engineering from Mankato State University, Mankato, MN.

Major Kent T. Jones received his commission into the Minnesota National Guard as an Infantry Officer in June 1988. He was assigned as Fire Support Team Chief in Headquarters/Headquarters Company 2/135th Infantry (Artic Light). In July 1989 he was commissioned into the Regular United States Army as a Chemical Officer.

His first assignment after completing the Chemical Officer Basic Course was as Battalion Chemical Officer, 5/8 Infantry, 8th Infantry Division, Mainz, Germany. He was reassigned as NBC Decontamination Platoon Leader, 22nd Chemical Company, DISCOM, 3rd Armored Division, where he deployed and participated in operations Desert Storm and Desert Shield. Upon redeployment he was reassigned as Chemical Reconnaissance Platoon Leader, 25th Chemical Company, 1/1 Cavalry, 1st Armored Division, where he deployed to operation Desert Fox as Chemical Detachment Commander, TF 3/77 Armor, 8th Infantry Division. Upon redeployment he was again reassigned as Division Mechanized Smoke Platoon Leader, 25th Chemical Company.

In July 1993 Major Jones attended the Chemical Officer Advanced Course and after graduation was assigned as commander, 89th Chemical Company, 3rd Armored Cavalry Regiment, Fort Bliss, Texas. While serving with the 3rd ACR he also commanded the Regimental Headquarters/Headquarters Troop and served as Regimental

Chemical Officer. In September 1996 he was reassigned as Brigade Chemical Officer 108th Air Defense Artillery Brigade (Airborne).

In June 1997 he was assigned as Chemical Team Chief, 278th Training Squadron, 1st U.S. Army where he served until August 1999 when he entered the School of Engineering, Air Force Institute of Technology, Wright-Patterson Air Force Base where he is currently serving.

REPORT DOCUMENTATION PAGE				Form Approved OMB No. 074-0188	
<p>The public reporting burden for this collection of information is estimated to average 1 hour per response, including the time for reviewing instructions, searching existing data sources, gathering and maintaining the data needed, and completing and reviewing the collection of information. Send comments regarding this burden estimate or any other aspect of the collection of information, including suggestions for reducing this burden to Department of Defense, Washington Headquarters Services, Directorate for Information Operations and Reports (0704-0188), 1215 Jefferson Davis Highway, Suite 1204, Arlington, VA 22202-4302. Respondents should be aware that notwithstanding any other provision of law, no person shall be subject to an penalty for failing to comply with a collection of information if it does not display a currently valid OMB control number.</p> <p>PLEASE DO NOT RETURN YOUR FORM TO THE ABOVE ADDRESS.</p>					
1. REPORT DATE (DD-MM-YYYY) 04-03-2002		2. REPORT TYPE Master's Thesis		3. DATES COVERED (From – To) Aug 2001 – March 2002	
4. TITLE AND SUBTITLE MEASUREMENTS OF NEUTRON INDUCED SURFACE AND BULK DEFECTS IN 4H SILICON CARBIDE				5a. CONTRACT NUMBER	
				5b. GRANT NUMBER	
				5c. PROGRAM ELEMENT NUMBER	
6. AUTHOR(S) Kent T. Jones, Major, USA				5d. PROJECT NUMBER	
				5e. TASK NUMBER	
				5f. WORK UNIT NUMBER	
7. PERFORMING ORGANIZATION NAME(S) AND ADDRESS(ES) Air Force Institute of Technology Graduate School of Engineering and Management (AFIT/EN) 2950 P Street, Building 640 WPAFB OH 45433-7765				8. PERFORMING ORGANIZATION REPORT NUMBER AFIT/GNE/ENP/02M-03	
9. SPONSORING/MONITORING AGENCY NAME(S) AND ADDRESS(ES) Air Force Institute of Technology Graduate School of Engineering and Management (AFIT/EN) 2950 P Street, Building 640 WPAFB OH 45433-7765				10. SPONSOR/MONITOR'S ACRONYM(S)	
				11. SPONSOR/MONITOR'S REPORT NUMBER(S)	
12. DISTRIBUTION/AVAILABILITY STATEMENT APPROVED FOR PUBLIC RELEASE; DISTRIBUTION UNLIMITED.					
13. SUPPLEMENTARY NOTES					
14. ABSTRACT <p>The effects of neutron irradiation was investigated in both n- and p-type 4H silicon carbide. Photoluminescence (PL), deep level transient spectroscopy (DLTS), and Hall effect measurements where used to observe optical and electrical characteristics and identify changes in basic material properties. The material was irradiated using an open pool research reactor. Highly doped n- and p-type materials ($N_D-N_A \sim 1.2E17$ and $N_A-N_D \sim 1.5E18 \text{ cm}^{-3}$ respectively) were chosen to aid in device fabrication.</p> <p>The material demonstrated no measurable effect to 1 MeV neutrons at fluences of up to $1E14 \text{ n/cm}^2$ and devices were unable to be constructed when exposed to fluences greater then $1E16 \text{ n/cm}^2$. The effective suppression of the near bandgap zero phonon PL luminescence lines was shown as a function of increasing neutron fluence, and attributed to the dislocation of neutral nitrogen donors. Deep level defects sites also developed and where shown to increase in density with increased neutron fluence. Hall measurements generally agreed with theoretical expectations but failed to yield conclusive results. Capacitance rollover was observed near 510 K beginning with fluences of around $5E15 \text{ n/cm}^2$. Irradiated devices also showed unexpectedly permanent degradation after hour-long exposure to temperatures exceeding 600K during DLTS measurements.</p>					
15. SUBJECT TERMS 4H- Silicon Carbide, Neutron, Photoluminescence, Deep Level Transient Spectroscopy, Hall Effect, Schottky Diode, and Radiation Hardness					
16. SECURITY CLASSIFICATION OF:			17. LIMITATION OF ABSTRACT UU	18. NUMBER OF PAGES 108	19a. NAME OF RESPONSIBLE PERSON LTC James C. Petrosky, ENP
a. REPORT U	b. ABSTRACT U	c. THIS PAGE U			19b. TELEPHONE NUMBER (Include area code) (937) 255-3636, ext 4600